PALEOCEANOGRAPHY, VOL. 24, PA2215, doi:10.1029/2008PA001685, 2009

Early to middle Eocene history of the Arctic Ocean from Nd-Sr isotopes in fossil fish debris, Lomonosov Ridge

J. D. Gleason,[1] D. J. Thomas,[2] T. C. Moore Jr.,[1] J. D. Blum,[1] R. M. Owen,[1] and B. A. Haley[3]

Received 9 September 2008; revised 25 January 2009; accepted 8 April 2009; published 5 June 2009.

[1] Strontium and neodymium radiogenic isotope ratios in early to middle Eocene fossil fish debris (ichthyoliths) from Lomonosov Ridge (Integrated Ocean Drilling Program Expedition 302) help constrain water mass compositions in the Eocene Arctic Ocean between ~55 and ~45 Ma. The inferred paleodepositional setting was a shallow, offshore marine to marginal marine environment with limited connections to surrounding ocean basins. The new data demonstrate that sources of Nd and Sr in fish debris were distinct from each other, consistent with a salinity-stratified water column above Lomonosov Ridge in the Eocene. The $^{87}Sr/^{86}Sr$ values of ichthyoliths (0.7079–0.7087) are more radiogenic than Eocene seawater, requiring brackish to fresh water conditions in the environment where fish metabolized Sr. The $^{87}Sr/^{86}Sr$ variations probably record changes in the overall balance of river Sr flux to the Eocene Arctic Ocean between ~55 and ~45 Ma and are used here to reconstruct surface water salinity values. The ε_{Nd} values of ichthyoliths vary between −5.7 and −7.8, compatible with periodic (or intermittent) supply of Nd to Eocene Arctic intermediate water (AIW) from adjacent seas. Although the Norwegian-Greenland Sea and North Atlantic Ocean were the most likely sources of Eocene AIW Nd, input from the Tethys Sea (via the Turgay Strait in early Eocene time) and the North Pacific Ocean (via a proto-Bering Strait) also contributed.

Citation: Gleason, J. D., D. J. Thomas, T. C. Moore Jr., J. D. Blum, R. M. Owen, and B. A. Haley (2009), Early to middle Eocene history of the Arctic Ocean from Nd-Sr isotopes in fossil fish debris, Lomonosov Ridge, *Paleoceanography*, *24*, PA2215, doi:10.1029/2008PA001685.

1. Introduction

[2] The Arctic Ocean (Figure 1) plays an important role in modulating global climate through atmosphere-ocean heat exchange and by driving the thermohaline circulation of the world ocean [e.g., *Aagaard and Carmack*, 1989, 1994, and references therein]. Freshwater exchange between the Arctic and adjacent Greenland-Norwegian Sea strongly influences convective overturn and the formation of North Atlantic Deep Water (NADW), while variation in the NADW strength may have a strong impact on both long-term regional and global climate [*Broecker et al.*, 1985]. High-latitude regions themselves are also very sensitive to global climate change, as indicated by models for future global warming driven by atmospheric CO_2 buildup [e.g., *Dai et al.*, 2001]; thus, understanding how high latitudes respond to global warming has powerful implications for forecasting future climate. Current projections of future warming predict global average temperatures comparable to the warmest climates of the past 60 million years within just 200 years [e.g., *Crowley and Kim*, 1995], but these models require constant refinement as new data are obtained. The warmest of these "climate optima" occurred during the early Eocene, a period that coincided with a very high level of atmospheric CO_2 [*Zachos et al.*, 2001; *Pearson and Palmer*, 2000; *Pagani et al.*, 2005; *Sluijs et al.*, 2008a]. While it is generally believed that an increased concentration of greenhouse gases in Earth's atmosphere should diminish the rate of heat loss from the Earth's climate system in general [e.g., *Sloan et al.*, 1992; *Sloan and Rea*, 1996; *Crowley and Zachos*, 2000], the impact of such extreme warmth on the Arctic region [e.g., *Jahren and Sternberg*, 2003], and particularly on the climate feedbacks associated with the Arctic Ocean, are not well constrained at this time. This paper reports results of a neodymium and strontium radiogenic isotope investigation on early and middle Eocene fish debris recovered at Lomonosov Ridge (IODP Expedition 302) in the central Arctic Ocean, with implications for the paleoceanographic and paleoclimatic development of the Arctic during the early Eocene climatic optimum.

2. Paleo-Arctic Ocean Basin

[3] Detailed knowledge of the tectonic and oceanographic development of the Arctic Ocean has historically been quite poor relative to the other major ocean basins [*Bukry*, 1984; *Marincovich et al.*, 1990; *Johnson et al.*, 1994; *Iakovleva et al.*, 2001]. Permanent ice cover in the central Arctic Ocean

[1]Department of Geological Sciences, University of Michigan, Ann Arbor, Michigan, USA.
[2]Department of Oceanography, Texas A&M University, College Station, Texas, USA.
[3]Leibniz Institute of Marine Sciences at University of Kiel (IFM-GEOMAR), Kiel, Germany.

0883-8305/09/2008PA001685$12.00

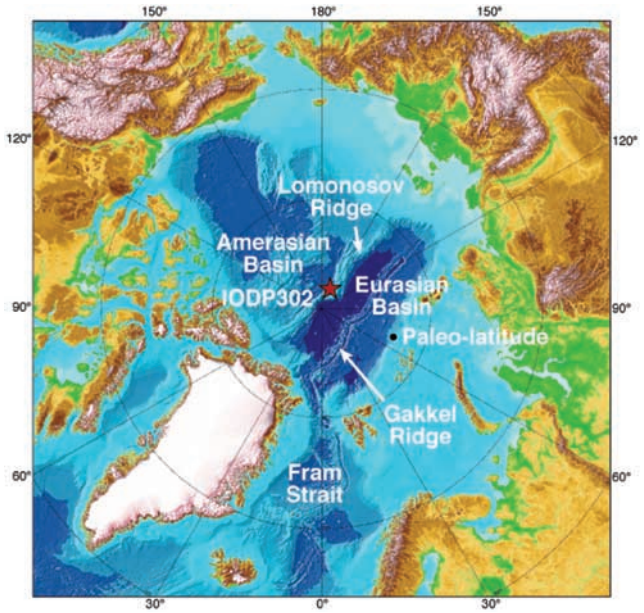

Figure 1. The modern Arctic Ocean Basin (modified from *Jakobsson et al.* [2000]) with IODP Expedition 302 drill sites at Lomonosov Ridge shown (57 Ma paleoposition from *Moran et al.* [2006]). Lomonosov Ridge is a rifted ribbon fragment of the pre-57 Ma Eurasian continental margin [*Moran et al.*, 2006]. Seafloor spreading along Gakkel Ridge generated post-57 Ma seafloor of the Eurasian Basin.

has rendered recovery of continuous and long sediment records impossible until only recently. Our understanding of the tectonic and paleoclimatic history of the Arctic Ocean increased tremendously upon completion of the Integrated Ocean Drilling Program (IODP) Arctic Coring Expedition (ACEX) in the summer of 2004 [*Moran et al.*, 2006; *Expedition 302 Scientists*, 2005, 2006; *Backman and Moran*, 2008]. The success of this drilling expedition has allowed the scientific community to begin to address the following questions directly: When did the Arctic become an ice-covered ocean? What was the balance of runoff, precipitation and evaporation during times when the Arctic was seasonally free of ice? When did thermal subsidence of the Greenland-Faroe Ridge and the tectonic widening of the Fram Strait (Figure 1) allow effective exchange and circulation of waters between the Arctic and the North Atlantic? One of the important primary discoveries from IODP Leg 302 was evidence that Arctic ice first appeared as early as the middle Eocene [*St. John*, 2008; *Moran et al.*, 2006], indicating a parallel cooldown with the Antarctic region [e.g., *Zachos et al.*, 2001]; however, the influence of this transition on circulation in the Arctic Basin remains unknown.

[4] Recent studies now argue for a deep-water connection between the Arctic and the North Atlantic starting in the early Miocene [e.g., *Jakobsson et al.*, 2007], but we do not yet know how, or even if, the ancient Arctic Ocean renewed its bottom waters, or even to what extent the ancient Arctic Ocean was integrated with global ocean circulation. Tectonic reconstructions of the early Paleogene Arctic [*Lawver et al.*, 2002; *Thiede and Myhre*, 1996] have suggested that deep-water exchange between the Arctic and the world ocean was much more restricted than it is today. There was probably a shallow intermittent connection between Tethys and the Arctic via the western Siberian seaway (Turgay Strait [*Radionova et al.*, 2003]) through the end of early Eocene time (Figure 2), and possibly into the early part of the middle Eocene [*Onodera et al.*, 2008]. The water depth of this connection is unknown; however, with the lack of any significant land ice during the warmest part of the Eocene, sea level may have been 70–80 m higher than it is today [*Miller et al.*, 2005a]. The complicated assembly of lithospheric slivers in far eastern Siberia also leaves open the possibility of a connection with the Pacific Ocean during this time [*Lawver et al.*, 2002] (see also http://www.odsn.de/). Shallow connections with the Atlantic probably existed off and on through the middle Eocene, becoming more established by 45 Ma [*Onodera et al.*, 2008]. Therefore, shallow water connections with the Atlantic, Pacific and Tethys could all have existed at various times during the early Eocene (Figure 2), and some combination of these may have persisted well into the middle and even late Eocene,

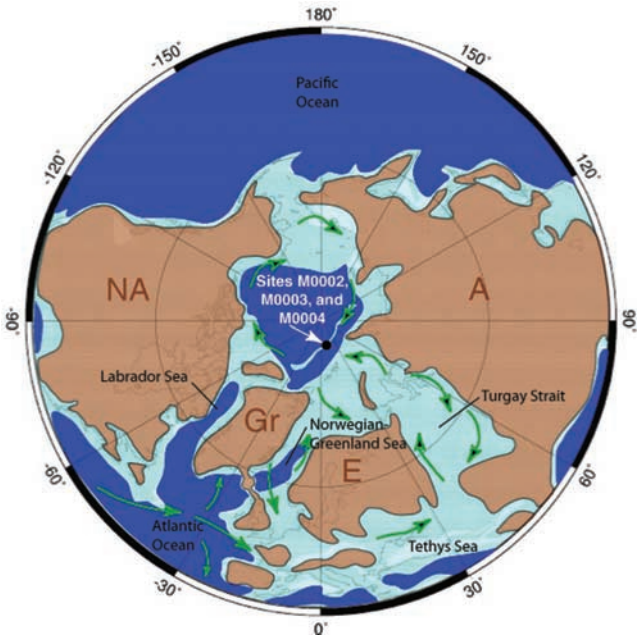

Figure 2. The 50 Ma paleoreconstruction of the early Eocene Arctic Ocean Basin showing position of IODP 302 drill sites (modified from *Expedition 302 Scientists* [2005]). Possible shallow marine connections existed between the Arctic and Tethys (via western Siberian Seaway/Turgay Strait), North Atlantic (via the Norwegian-Greenland Sea and the Labrador Sea), and the Pacific Ocean (via proto-Bering Strait). NA, North America; A, Asia/Siberia; Gr, Greenland; E, Europe. Middle Eocene connections are uncertain, and exchange with Tethys may have ceased by early middle Eocene time [*Radionova et al.*, 2003; *Radionova and Khokhlova*, 2000].

on the basis of the occurrence of siliceous microfossil assemblages [*Onodera et al.*, 2008].

3. Samples Recovered by IODP Arctic Coring Expedition 302

[5] Lomonosov Ridge preserves a history of sedimentation dating back to the Late Cretaceous when it was still joined with continental Eurasia [*Backman et al.*, 2006; *Moore and Expedition 302 Scientists*, 2006; *O'Regan et al.*, 2008]. It represents a sliver of thinned and submerged continental crust in the central Arctic Ocean that rifted from continental Eurasia ~57 million years ago, migrating slowly away via seafloor spreading at the Gakkel Ridge (Figure 1) and accumulating more than 400 m of postrift marine pelagic sediment [*Moran et al.*, 2006; *Moore and Expedition 302 Scientists*, 2006; *Backman et al.*, 2006, 2008; *Backman and Moran*, 2008]. Four IODP 302 drill sites were cored atop Lomonosov Ridge at ~1,200 m water depth (Sites M0002 through M0004) near 88°N, resulting in a 428 m composite sedimentary section [*Backman et al.*, 2008] consisting of the following main lithologic age units, from oldest to youngest: (1) Late Cretaceous shallow marginal marine sediments (ACEX Lithostratigraphic Unit 4), separated by angular unconformity from; (2) a late Paleocene through early and middle Eocene section of variably organic-rich, sulfide-bearing, partly microlaminated biosiliceous clay and silty clay (ACEX Lithostratigraphic Units 3 and 2 and Lithostratigraphic Subunit 1/6); (3) a highly condensed, or missing, interval from ~44 to ~17.5 Ma; and (4) brown oxidized, silty clays containing abundant ice rafted debris of Neogene age (ACEX Lithostratigraphic Subunits 1/1–1/4) with a transitional subunit (1/5) of Miocene age, all <17.5 Ma [*Expedition 302 Scientists*, 2005, 2006; *Moran et al.*, 2006; *Moore and Expedition 302 Scientists*, 2006; *Jakobsson et al.*, 2007; *Backman et al.*, 2008]. Details of the ACEX lithostratigraphy can be found online in the IODP Proceedings Volume 302 http://publications.iodp.org/proceedings/302/302toc.htm), and in papers from the 2008 ACEX special section "Cenozoic Paleoceanography of the Central Arctic Ocean" in *Paleoceanography*, *23*(1), 2008 [see *Backman and Moran*, 2008].

[6] The focus of this study is the section spanning a ~10 Ma interval from the Paleocene/Eocene Thermal Maximum (PETM) at ~55 Ma (ACEX Lithostratigraphic Unit 3) to the middle Eocene section above the hiatus (ACEX Lithostratigraphic Subunit 1/6) at ~45 Ma. The Arctic PETM is identified by the presence of the dinoflagellate cyst *Apectodinium augustum* [*Expedition 302 Scientists*, 2006; *Sluijs et al.*, 2006, 2008a] accompanied by a characteristic $\delta^{13}C_{org}$ minimum [*Stein et al.*, 2006; *Pagani et al.*, 2006; *Sluijs et al.*, 2006]. Spore remains of the floating freshwater hydropterid fern *Azolla* are superabundant in the 49–48.3 Ma interval, marking the lower/middle Eocene boundary [*Expedition 302 Scientists*, 2006; *Moran et al.*, 2006; *Brinkhuis et al.*, 2006]. These remains are interpreted as autochthonous, that is, produced over a large area of the Arctic Ocean at a time when very low salinity conditions dominated the surface environment [*Brinkhuis et al.*, 2006; *Stein et al.*, 2006]. Biosiliceous biostratigraphic markers are abundant in the Eocene record, and include mostly low-salinity-tolerant organic-walled dinoflagellate cysts, diatoms, ebridians and silicoflagellates, particularly in the middle Eocene interval [*Onodera et al.*, 2008; *Stickley et al.*, 2008]. Radiolaria and biogenic carbonate are rare to absent in this part of the section, indicative of an overall low-salinity environment during the early and middle Eocene and lack of open marine conditions [*Expedition 302 Scientists*, 2006; *Brinkhuis et al.*, 2006; *Moran et al.*, 2006; *Onodera et al.*, 2008; *Stickley et al.*, 2008].

[7] Early results from IODP Arctic Coring Expedition 302 (ACEX) have demonstrated that during early and middle Eocene time, Lomonosov Ridge was a shallow but rapidly subsiding bathymetric high with paleodepths of between 250 and 600 m [*Moore and Expedition 302 Scientists*, 2006] (see *O'Regan et al.* [2008] for a different interpretation). Eocene sedimentation rates were comparable to current rates in the central Arctic Basin (~10–25 mm/ka [*Pälike et al.*, 2008; *Sangiorgi et al.*, 2008a]), with astronomically modulated depositional cycles indicated by well-preserved microlaminar banding in parts of the early and middle Eocene section [*Pälike et al.*, 2008]. Extensive work on the organic component has revealed peak mean sea surface temperatures (SST) during the ~55 Ma Paleocene-Eocene Thermal Maximum (PETM) of 23°C [*Sluijs et al.*, 2006, 2008a; *Pagani et al.*, 2006], and summer air temperatures as high as ~25°C [*Weijers et al.*, 2007], indicating a mild, temperate climate. By earliest middle Eocene time (i.e., 49–48.3 Ma *Azolla* event), sea surface temperatures were cooler, but still 10–13°C higher than the modern Arctic according to estimates [*Brinkhuis et al.*, 2006; *Weller and Stein*, 2008]. The first evidence for sea ice formation in the ACEX record is found within the late middle Eocene interval at ~46 Ma [*Moran et al.*, 2006; *Sangiorgi et al.*, 2008b; *St. John*, 2008]. Ice-rafted debris is a primary component of the posthiatus (post-17.5 Ma) ACEX record [*Expedition 302 Scientists*, 2006; *Jakobsson et al.*, 2007].

[8] According to several recent studies, early to middle Eocene oceanic anoxia at Lomonosov Ridge was initiated at the PETM around 55.5 Ma [*Stein et al.*, 2006; *Weller and Stein*, 2008; *Knies et al.*, 2008; *Sluijs et al.*, 2008a; *Backman et al.*, 2008], and likely persisted until ~44 Ma, possibly expanding into the photic zone of the water column at times [*Weller and Stein*, 2008]. Euxinic and/or oxygen depleted conditions in the Arctic were likely a result of several factors brought about by relative isolation from other oceans. Slow circulation, coupled with enhanced rainfall and continental runoff, may have established a nutrient "trap" [*Meyer and Kump*, 2008] which, in concert with unprecedented warmth, allowed for times of extremely high surface water primary productivity and organic carbon flux through the water column, further depleting waters of their dissolved oxygen content [*Pagani et al.*, 2006; *Weller and Stein*, 2008; *Knies et al.*, 2008; *Sluijs et al.*, 2008a; *Spofforth et al.*, 2008]. Total organic carbon (TOC) for early and middle Eocene ACEX sediments and the PETM varies from 1 to 5%, with a significant component of marine algal carbon particularly in the middle Eocene [*Stein et al.*, 2006]. Low but variable salinity conditions at the surface of the Arctic Ocean during the PETM and early and middle

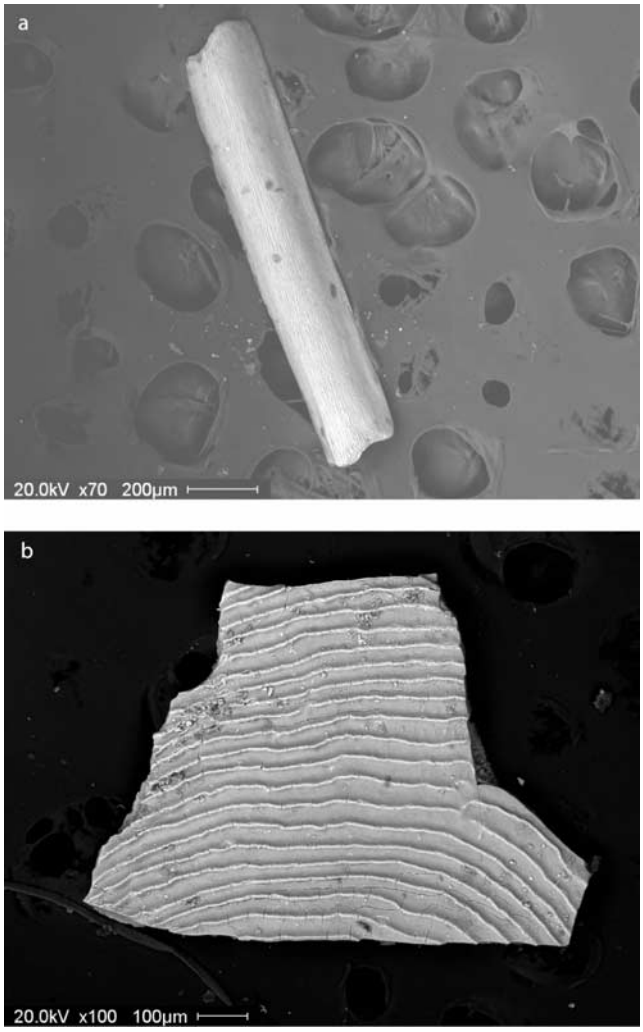

Figure 3. SEM images of (a) middle Eocene fish bone and (b) scale material analyzed from IODP Leg 302 core samples. The scale fragments show growth bands characteristic of smelt, a small fish that commonly inhabits productive, brackish water environments (G. Smith, University of Michigan, personal communication, 2005).

Eocene time are indicated through several lines of evidence, including oxygen isotope paleosalinity estimates [*Waddell and Moore*, 2008], the occurrence of freshwater species such as *Azolla* (49–48.3 Ma), and by proportionally higher abundances of other low-salinity-tolerant species [*Brinkhuis et al.*, 2006; *Moran et al.*, 2006; *Stickley et al.*, 2008; *Onodera et al.*, 2008]. Between 49 and 48.3 Ma, proliferation and dispersal of the fresh water fern *Azolla* occurred in the Arctic Ocean, forming a reliable time stratigraphic marker for the base of the middle Eocene [*Brinkhuis et al.*, 2006]. This event coincided with rapidly falling sea level and diminishing exchange between Arctic surface waters and the Norwegian-Greenland Sea [*Miller et al.*, 2005a; *Brinkhuis et al.*, 2006].

[9] In this contribution to the rapidly growing body of work based on the ACEX sediment record, we attempt to explore further the nature of Arctic Basin hydrography, circulation and water exchange during the Eocene through proxy records of the neodymium (Nd) and strontium (Sr) radiogenic isotopic compositions recorded in fossil fish debris. Anoxic conditions during early and middle Eocene time resulted in extraordinary preservation of phosphatic fish teeth, scales and bone fragments of one or more species of Arctic Ocean smelt in sediments at the drill site (Figure 3). These geochemical records potentially allow reconstruction of some of the properties of the water column overlying the Lomonosov Ridge during the early and middle Eocene. The Sr isotopic data are consistent with a very low salinity surface environment during the early and middle Eocene, when extreme warmth, productivity and anoxia dominated the Arctic Ocean [*Moran et al.*, 2006; *Sluijs et al.*, 2006; *Brinkhuis et al.*, 2006; *Stein et al.*, 2006]. Evidence of intermittent exchange between the Arctic and adjacent oceans is also preserved in the deeper water (Nd) isotope signature of the fish debris, although limited connections during the Eocene probably restricted this exchange. We conclude that an active year-round Arctic hydrologic cycle, along with eustatic and tectonic controls on oceanic exchange, must have exerted significant control on the evolution of Eocene Arctic Ocean water column structure and the isotopic composition of early and middle Eocene fish debris reported on here.

4. Sr and Nd Isotope Marine Geochemistry

[10] Nd and Sr radiogenic isotopes are widely used in marine studies as proxy indicators for the origin and composition of paleo water masses [e.g., *Frank*, 2002; *Goldstein and Hemming*, 2003]. The Sr isotopic composition of the global seawater reservoir at any point in geologic time reflects the integration of inputs from terrestrial weathering, seafloor hydrothermal activity and carbonate remobilization [*Palmer and Edmond*, 1989]. The $^{87}Sr/^{86}Sr$ value of well-mixed (open) ocean waters will be the same everywhere at any given time, because of the long residence time of Sr (~3 million years) relative to oceanic mixing rates (~1500 years) [*Richter and Turekian*, 1993]. The Sr in fossilized teeth and bones of marine fish records the $^{87}Sr/^{86}Sr$ composition of the seawater in which the organisms lived, generally from waters within the photic zone (the fish bones, scales and teeth employed in this study represent a variety of Eocene Arctic smelt (G. Smith, University of Michigan, personal communication, 2005)). In the open ocean, fossilized fish debris (ichthyoliths) typically retain the Sr isotopic composition of the global ocean signature at the time they were deposited, and in that environment the Sr isotopic composition of ancient fish debris can be used as a chronometer [*Ingram*, 1995; *Martin and Haley*, 2000; *Martin and Scher*, 2004; *Gleason et al.*, 2002, 2004]. In the case of restricted marine basins like the Eocene Arctic Ocean, the Sr isotopic composition might be expected to record compositions different from that of the global seawater value. For example, in marginal marine settings and estuaries, this approach has found utility as a proxy for paleosalinity [e.g., *Schmitz et al.*, 1991; *Ingram and DePaolo*, 1993; *Holmden et al.*, 1997]. Care must be

taken to properly clean ichthyoliths of any surface contaminants, and to evaluate them for any evidence of possible Sr gain (diagenetic uptake) from surrounding pore waters that might compromise their value as a seawater proxy [*Ingram*, 1995; *Martin and Scher*, 2004; *Gleason et al.*, 2002, 2004].

[11] In contrast to Sr, the Nd isotopic composition of seawater is dictated solely by weathering inputs to the sea [e.g., *Goldstein and Jacobsen*, 1988; *Elderfield et al.*, 1990; *Halliday et al.*, 1992]. Seawater Nd isotope values, expressed as ε_{Nd} (the $^{143}Nd/^{144}Nd$ value of a geologic sample normalized to the accepted bulk earth value [*DePaolo and Wasserburg*, 1976]), demonstrate distinct intrabasinal and interbasinal variations at any given time because of (1) differences in ages, compositions and weathering of subaerially exposed rocks supplying Nd to a given ocean basin [e.g., *Piepgras and Wasserburg*, 1987; *Piepgras and Jacobsen*, 1988; *Goldstein and Jacobsen*, 1988; *Jeandel*, 1993; *Amakawa et al.*, 2000] and (2) the short oceanic residence time (<1000 years) of Nd relative to oceanic mixing rates [e.g., *Tachikawa et al.*, 1999]. The Nd isotopic composition of individual water masses is therefore derived from the integrated Nd flux of all dissolved materials draining into the water mass source region from the continental margins [*Goldstein and Jacobsen*, 1988; *Elderfield et al.*, 1990; *Sholkovitz*, 1993; *Jeandel et al.*, 2007]. Because the teeth and bones of living fish incorporate no significant Nd into their structure, their ecology/lifecycle has no bearing on the ε_{Nd} composition of fossilized (= ichthyolith) teeth and bones [e.g., *Wright et al.*, 1984; *Staudigel et al.*, 1985]. Instead, ichthyoliths acquire their Nd composition through rapid postmortem uptake at the sediment/water interface [e.g., *Staudigel et al.*, 1985; *Reynard et al.*, 1999] via adsorption and substitution mechanisms while still on the seafloor [e.g., *Grandjean and Albaréde*, 1989; *Reynard et al.*, 1999]. Thus, this biogenic phosphate (i.e., carbonate fluorapatite) should faithfully record the average Nd isotopic composition of waters flowing across the seafloor over very short duration time spans (e.g., hundreds to thousands of years) [e.g., *Wright et al.*, 1984; *Shaw and Wasserburg*, 1985; *Staudigel et al.*, 1985; *Martin and Haley*, 2000; *Martin and Scher*, 2004; *Thomas*, 2005]. Relevant to this study is the fact that previous investigations have already demonstrated that fish bones and scales record and preserve the same Nd isotopic signal as fish teeth in the marine environment [*Thomas and Via*, 2007].

5. Methods

[12] We obtained samples spanning approximately 10 million years of early and middle Eocene sedimentation in the central Arctic Basin from IODP 302 cores MOO2A and MOO4A [*Backman et al.*, 2008]. For samples processed at the University of Michigan (UM) and University of North Carolina (UNC), fossil fish debris (including well-preserved scales, teeth and bone fragments) was hand picked from several milligrams of material (Figure 3). Samples were first rinsed and ultrasonicated in microcentrifuge tubes with deionized water multiple times to remove any loosely adhering contaminants [*Waddell and Moore*, 2008]. Because of highly reducing, opaque organic and carbon-rich coatings (Figure 3), the methods routinely employed for cleaning open marine highly oxidized fossil fish teeth and other microfossils (e.g., the aggressive reductive cleaning techniques modified from *Boyle* [1981]) had to be adapted to include a more aggressive oxidizing procedure. The samples were subjected to an intensive multistep oxidizing treatment using hot (low blank Suprapur) hydrogen peroxide (H_2O_2), followed by thorough cleaning and rinsing with dilute (Seastar) acetic acid and ultradilute (Seastar) nitric acid. Toward the end of the study, several leach fractions were obtained from hot solutions of Suprapur H_2O_2 which produced enough Sr and Nd derived from the organic-rich coatings to measure isotopic compositions. All fish debris (e.g., residues of the cleaning process) were digested in 3 N Seastar nitric acid, followed by low blank ion exchange chromatography at the UM to separate Sr and REE from the matrix for isotope ratio mass spectrometry. Sr-Spec (Eichrom) resin in miniaturized columns was employed to extract Sr, resulting in blanks lower than 100 pg (<1/1000 total Sr analyzed) and recovery of >200 nanograms Sr in most cases. Sr yields were monitored periodically by ICP analysis [*Gleason et al.*, 2004]. Sr isotopic ratios were obtained at UM by thermal ionization mass spectrometry [*Gleason et al.*, 2002, 2004] on a Finnigan MAT equipped with 8 collectors using both static and dynamic analysis. The NBS-987 isotopic standard gave a mean value of $^{87}Sr/^{86}Sr = 0.710246 \pm 12$ (n = 28) over the course of this study, requiring no corrections to the data.

[13] Rare earth elements (REE, e.g., Nd) were chemically separated from the non-Sr fraction as a group using disposable RE-Spec resin (Eichrom), employing the same miniaturized columns used for Sr at the UM. Nd was then chromatographically separated from the other REE using the 2-methyllactic acid method at the UNC [*Thomas et al.*, 2003] for isotopic analysis. $^{143}Nd/^{144}Nd$ isotopic ratios were obtained on ~300 mV NdO^+ beams at the UNC on a GV Sector 54 thermal ionization mass spectrometer. External analytical precision based upon replicate analysis of the international standard JNd_i [*Tanaka et al.*, 2000] yielded 0.512111 ± 0.000010 (2 s) (n = 30), which is calibrated relative to the accepted La Jolla standard value of 0.511858 (= 0.512116 JNd_i). The total procedural blank for Nd was ~15 pg and considered negligible compared to sample yields.

[14] Additional leaching experiments were carried out at GEOMAR (Kiel) by a different method on a small subset of bulk sedimentary samples following methods of *Haley et al.* [2008a, 2008b]. After Milli-Q rinsing, a dilute solution of hydroxylamine, HCl and acetic acid buffered to pH of 4 with NaOH was leached from 0.5 g of sediment, dried down and processed through conventional AG 50W-X12 ion exchange resin for separation of Sr and REE from the matrix. Nd was further purified using conventional HDEHP chromatography, and analyzed (as Nd+) for isotopic composition at GEOMAR using a Thermo Triton TIMS [*Haley et al.*, 2008b]. External reproducibility (2 SE) of $^{143}Nd/^{144}Nd$ ratios is 0.50 epsilon units. $^{87}Sr/^{86}Sr$ was measured at GEOMAR using an Axiom MC-ICPMS [*Haley et al.*, 2008b]. External (2 SE) reproducibility of $^{87}Sr/^{86}Sr$

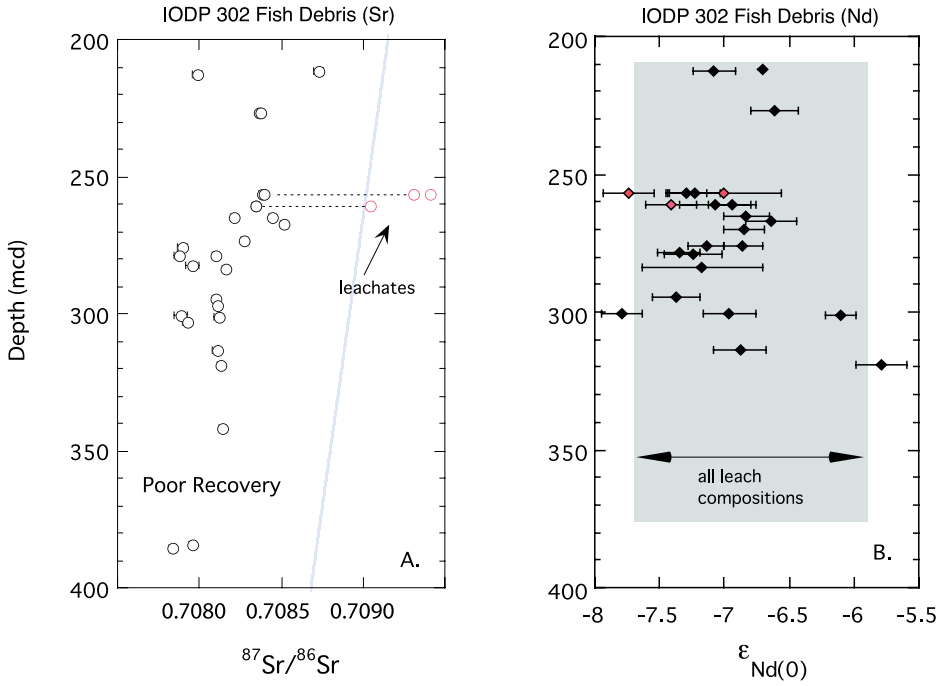

Figure 4. (a) Sr and (b) Nd isotopic variations in Lomonosov Ridge early and middle Eocene fish debris plotted against depth (mcd) from IODP Leg 302. All plotted symbols represent fish debris and leachates analyzed from Table 1. In Figure 4a the three plotted leachate data points (red symbols) represent H_2O_2 leachates of fish debris (Table 1). Leachate $^{87}Sr/^{86}Sr$ data obtained by different methods (Table 2) all plot to the right of the gray line in Figure 4a, indicating that all leachate Sr is more radiogenic than the H_2O_2-treated (residue) material. In Figure 4b, the $\varepsilon_{Nd(0)}$ of H_2O_2-treated fish debris overlap in composition with the three plotted H_2O_2-leachate data points (red symbols) from Table 1. Leachate $\varepsilon_{Nd(0)}$ values obtained by different methods (Table 2) all plot within the gray field in Figure 4b, overlapping the $\varepsilon_{Nd(0)}$ of the H_2O_2-treated (residue) material. Depth intervals ~340–380 mcd are characterized by sparse core recovery [*Backman et al.*, 2008].

was 0.000031. Total procedural blanks were <3 ng Sr and negligible for Nd. These measurements are included for comparison with the leaching experiments done at Michigan, and also to fill gaps in the early Eocene Nd record.

6. Age Model

[15] The age model used for the samples presented here is that published by *Backman et al.* [2008], and is the same as that employed for papers published in the ACEX special section in *Paleoceanography* [see *Backman and Moran*, 2008]. The early and middle Eocene age-depth curve is based primarily on dinocyst stratigraphy and some biosiliceous microfossil age datums, with extrapolation across unrecovered intervals using assumptions involving sedimentation rates [*Backman et al.*, 2008] and the precisely determined datums at 55 Ma (PETM) and the 49 Ma base for the middle Eocene identified by the presence of *Azolla*.

7. Results

7.1. Sr Isotopic Data

[16] $^{87}Sr/^{86}Sr$ ratios for chemically cleaned and H_2O_2-treated early and middle Eocene ichthyoliths at Lomonosov Ridge (Table 1 and Figure 4a) range from 0.7078 (385.25 mcd; 55 Ma PETM) to 0.7088 (211.72 mcd; 45 Ma). These data suggests an overall trend toward more radiogenic compositions in younger samples, although considerable variation exists within this trend (Figure 4a). For example, most of this range exists within a narrow interval at ~45 Ma which is characterized by the first appearance of ice-rafted debris in the ACEX record (Table 1). Three replicate analyses composed of a mixture of fish teeth, scales, bones and fish debris (including bone and scale fragments) from intervals 226.73 mcd, 256.61 mcd and 260.81 mcd (Table 1) show that different mixtures of ichthyolith material from a given interval yield identical values within error, lending confidence to our methods. Three H_2O_2-leachate Sr fractions (see Methods) are considerably more radiogenic (Figure 4a) than the residual phosphate (cleaned scale and bone fragment material) they are paired with (intervals 256.61 mcd and 260.81 mcd (Table 1)). The H_2O_2-leachate $^{87}Sr/^{86}Sr$ varies from 0.7090 to 0.7094 for these three analyses, and is representative of the Sr contained in the black, organic-rich coatings that are completely removed during hot hydrogen peroxide leaching (see methods). A duplicate H_2O_2-leach experiment using separate ichthyolith fractions (hand-picked fish scale and bone fragments) from interval 256.61 mcd shows that these leach fractions are similar in their Sr isotopic composition but slightly outside analytical error (Table 1), suggesting some heterogeneity in the

Table 1. IODP Leg 302 Eocene Fish Debris, Lomonosov Ridge: Nd-Sr Isotopic Compositions of Chemically Treated Fish Debris and H_20_2-Leach Fractions

Hole	Core	Section[a]	Top/Bottom	Depth (mcd)	Age[b] (Ma)	Sample Type	$^{87}Sr/^{86}Sr$[c]	2 SE ±	$^{143}Nd/^{144}Nd$[d]	2 SE ±	$\varepsilon_{Nd(0)}$[e]	2 SE ±	$^{147}Sm/^{144}Nd$[f]	$^{87}Rb/^{86}Sr$[f]
2A	48x	cc	139–151	211.72	44.960	fish debris	0.708725	0.000029	0.512293	0.000008	−6.70	0.15		
4B	3x	cc	bottom	212.71	45.000	fish debris	0.707986	0.000027	0.512275	0.000008	−7.08	0.16		
2A	52x	cc		226.73	45.580	fish tooth	0.708368	0.000020						
2A	52x	cc		226.73	45.580	bone fragments	0.708376	0.000016	0.512299	0.000009	−6.61	0.18		
2A	57x	2	102–104	246.00	46.370	untreated bone fragment							0.1480	
2A	58x residue a	cc	bottom	256.61	46.810	fish debris	0.708381	0.000013	0.512267	0.000010	−7.23	0.20	0.1409	0.0117
2A	58x residue b	cc	bottom	256.61	46.810	fish debris[g]	0.708398	0.000013	0.512265	0.000008	−7.29	0.16		
2A	58x leach a	cc	bottom	256.61	46.810	leach	0.709407	0.000013	0.512279	0.000023	−7.00	0.44	0.1383	0.0027
2A	58x leach b	cc	bottom	256.61	46.810	leach[g]	0.709309	0.000015	0.512241	0.000010	−7.74	0.20		
2A	59x	cc	0–2	260.81	46.990	scale fragments	0.708339	0.000016	0.512282	0.000009	−6.94	0.18		
2A	59x residue	cc	0–2	260.81	46.990	scale fragments[g]	0.708342	0.000013	0.512276	0.000014	−7.07	0.28		
2A	59x leach	cc	0–2	260.81	46.990	leach	0.709046	0.000015	0.512258	0.000010	−7.41	0.20		
2A	60x	cc		265.07	47.160	scale fragments	0.708440	0.000016	0.512288	0.000009	−6.83	0.18		
4A	4x	1	top 0–3	265.02	47.160	fish debris	0.708210	0.000021						
2A	61x	cc	4–6	267.22	47.250	scale fragments	0.708513	0.000017	0.512298	0.000010	−6.64	0.20		
4A	5x	1	82–84	270.00	47.360	fish debris			0.512287	0.000008	−6.85	0.16		
2A	62x	cc	4–6	273.51	47.510	1 large tooth	0.708270	0.000019						
4A	6x	2	82–84	275.83	47.610	fish debris	0.707892	0.000030	0.512286	0.000008	−6.86	0.15		
4A	6x	2	82–84	275.83	47.610	fish debris[g]			0.512272	0.000007	−7.14	0.14		
4A	6x	cc	bottom	278.78	47.730	2 fish teeth	0.708100	0.000022	0.512267	0.000011	−7.24	0.22		
4A	6x	cc	bottom	278.78	47.730	fish debris								0.0016
4A	7x	1	147–150	278.70	47.720	fish debris	0.707872	0.000027	0.512261	0.000008	−7.35	0.16		
4A	7x	cc		283.68	47.940	1 fish tooth	0.708159	0.000018	0.512271	0.000024	−7.17	0.46		
4A	8x	cc	bottom	282.58	47.880	1 fish tooth	0.707955	0.000043						
4A	10x	2	147–150	294.84	48.390	fish debris	0.708101	0.000018	0.512260	0.000009	−7.37	0.18		
4A	10x	cc	bottom	297.19	48.490	4 small teeth	0.708108	0.000017						
4A	11x *Azolla*	1	46–48	300.78	48.670	fish debris			0.512239	0.000008	−7.79	0.16		
4A	11x *Azolla*	3	46–48	300.78	48.670	fish debris	0.707886	0.000040	0.512281	0.000010	−6.96	0.20		
4A	12x *Azolla*	cc	bottom	301.37	48.710	fish debris	0.708118	0.000025	0.512325	0.000006	−6.10	0.12		
4A	11x *Azolla*	cc	bottom	302.73	48.800	fish debris	0.707923	0.000026						
4A	15x	cc	bottom	313.61	49.670	fish debris	0.708105	0.000024	0.512285	0.000010	−6.88	0.20		
4A	18x	cc	bottom	318.96	50.090	fish debris	0.708129	0.000021	0.512341	0.000010	−5.79	0.20		
4A	23x	1	top	341.60	51.870	fish debris	0.708141	0.000023						
4A	30x PETM	cc	bottom	384.54	55.150	fish debris	0.707958	0.000023						
4A	31x PETM	cc	bottom	385.25	55.190	fish debris	0.707833	0.000015						

[a]Here cc, core catcher.
[b]Age model from *Backman et al.* [2008].
[c]NBS987 $^{87}Sr/^{86}Sr = 0.710246 \pm 0.000012$ (n = 28; measured at University of Michigan).
[d]JNdi Nd standard measured at University of North Carolina was $^{143}Nd/^{144}Nd = 0.511211 \pm 10$ (2 SE; n = 30), calibrated to La Jolla value of $^{143}Nd/^{144}Nd = 0.511858$.
[e]Here $\varepsilon_{Nd(0)} = 10^4[(^{143}Nd/^{144}Nd_{sample})/(^{143}Nd/^{144}Nd_{chur}) - 1]$, where $^{143}Nd/^{144}Nd_{chur} = 0.512638$.
[f]Sm/Nd and Rb/Sr ratios measured by magnetic sector ICP-MS.
[g]Duplicated interval.

Table 2. Sr-Nd Isotopic Composition of Bulk Leach Fractions in Eocene Sediment From Lomonosov Ridge[a]

SPL Number	Leach Type[b]	Sample Name	Weight (g)	Depth (mcd)	Age[c] (Ma)	$^{87}Sr/^{86}Sr$	$^{143}Nd/^{144}Nd$	$\varepsilon_{Nd(0)}$[d]	$^{147}Sm/^{144}Nd$	$\varepsilon_{Nd(t)}$[e]	Latitude (deg)	Longitude (deg)	Water Depth (m)
111	DIW/10%leach	IODP 302: 2_46_2_70–72	0.5	199.84	44.47	0.709299					87.917	139.367	1209
144	DIW/10%leach	IODP 302: 2_49_2_68–70	0.5	210.84	44.93	0.711128	0.512269	−7.2		−7.0	87.917	139.367	1209
112	DIW/10%leach	IODP 302: 2_49_2_68–70	0.5	213.22	45.02	0.710931					87.917	139.367	1209
113	DIW/10%leach	IODP 302: 2_52_2_2–4	0.5	224.68	45.50	0.710480					87.917	139.367	1209
123	DIW/10%leach	IODP 302: 2_53_2_68–70	0.5	227.21	45.60	0.709821					87.917	139.367	1209
114	DIW/10%leach	IODP 302: 2_56_2_68–70	0.5	***240.92***	***46.16***	***0.710845***					87.917	139.367	1209
145	DIW/10%leach	IODP 302: 2_56_2_68–70	0.5	***240.92***	***46.16***	***0.710088***					87.917	139.367	1209
115	DIW/10%leach	IODP 302: 2_59_2_130–132	0.5	257.41	46.85	0.710754					87.917	139.367	1209
116	DIW/10%leach	IODP 302: 2_62_2_68–70	0.5	***269.80***	***47.36***	***0.710536***	0.512309	−6.4		−6.2	87.917	139.367	1209
146	DIW/10%leach	IODP 302: 2_62_2_68–70	0.5	***269.80***	***47.36***	***0.709411***					87.917	139.367	1209
117	DIW/10%leach	IODP 302: 4_7_2_70–72	0.5	276.79	47.64	0.708961					87.867	136.167	1288
118	DIW/10%leach	IODP 302: 4_10_2_68–70	0.5	293.54	48.10	0.709792					87.867	136.167	1288
147	DIW/10%leach	IODP 302: 4_10_2_68–70	0.5	294.04	48.14	0.709778	0.512279	−7.0		−6.7	87.867	136.167	1288
124	DIW/10%leach	IODP 302: 4_21_2_68–70	0.5	331.50	51.08	0.709650	0.512288	−6.8	0.1547	−6.5	87.867	136.167	1288
125	DIW/10%leach	IODP 302: 4_23_2_68–70	0.5	343.80	52.04	0.709312					87.867	136.167	1288
120	DIW/10%leach	IODP 302: 4_27_2_68–70	0.5	368.59	54.00	0.708857	0.512271	−7.2		−6.9	87.867	136.167	1288
148	DIW/10%leach	IODP 302: 4_27_2_68–70	0.5	369.59	54.07	0.708691	0.512297	−6.6		−6.3	87.867	136.167	1288

[a]Bold italic font denotes duplicate measurements of the same 3 cm interval.
[b]Leaching experiments conducted at GEOMAR by reductive cleaning methods (see text).
[c]Age-depth model from *Backman et al.* [2008].
[d]Here $\varepsilon_{Nd(0)} = 10^4[(^{143}Nd/^{144}Nd(t)_{sample})/(^{143}Nd/^{144}Nd(t)_{chur}) - 1]$ at sample age t = 0 Ma; $^{143}Nd/^{144}Nd(0)_{chur} = 0.512638$.
[e]Here $\varepsilon_{Nd(t)} = 10^4[(^{143}Nd/^{144}Nd(t)_{sample})/(^{143}Nd/^{144}Nd(t)_{chur}) - 1]$ at sample age t (Ma), using $^{143}Nd/^{144}Nd(0)_{chur} = 0.512638$, $^{147}Sm/^{144}Nd_{chur} = 0.1966$, and $^{147}Sm/^{144}Nd_{sample} = 0.1547$.

$^{87}Sr/^{86}Sr$ of the organic coatings. Regardless, these data emphasize the importance and effectiveness of the cleaning procedure for extracting viable "seawater" values from the Eocene ichthyolith material. A larger group of (non-H_2O_2) leachate $^{87}Sr/^{86}Sr$ analyses, generated by different methods (Table 2), also falls on a highly radiogenic trend (Figure 4a), overlapping the H_2O_2-leachate $^{87}Sr/^{86}Sr$ analyses. These (non-H_2O_2) leachate $^{87}Sr/^{86}Sr$ data (0.7087–0.711) also suggest a trend toward more radiogenic compositions in younger samples (Figure 4a). Rb/Sr ratios measured on a small subset of H_2O_2-leachate and residue samples (Table 1) reveal extremely low $^{87}Rb/^{86}Sr$ (<0.003), making age corrections for radiogenic ingrowth unnecessary. $^{87}Sr/^{86}Sr$ data reported here are therefore the measured, and not age-corrected, $^{87}Sr/^{86}Sr$ ratios (Tables 1 and 2). All $^{87}Sr/^{86}Sr$ ratios measured in this data set (Tables 1 and 2) are more radiogenic than the range reported for Eocene global seawater $^{87}Sr/^{86}Sr$ between 45 Ma and 55 Ma (0.7077–0.7078) by *McArthur et al.* [2001].

7.2. Nd Isotopic Data

[17] $\varepsilon_{Nd(0)}$ values in this data set represent the measured (present-day) $^{143}Nd/^{144}Nd$ ratios normalized to CHUR, or bulk earth (Tables 1 and 2). $\varepsilon_{Nd(0)}$ values for the chemically cleaned and H_2O_2-treated early and middle Eocene ichthyolith material (Table 1) vary from −5.8 (318.96 mcd; 50 Ma) to −7.8 (300.78 mcd; 48.7 Ma *Azolla*), showing no trends with stratigraphic position (Figure 4b). In fact, nearly the full $\varepsilon_{Nd(0)}$ range of the data set ($\Delta\varepsilon_{Nd}$ = 2) is found within the 4A 11x–12x *Azolla* interval (Table 1 and Figure 4b) at stratigraphic level 301.37–300.78 mcd (~48.7 Ma). Above level 300.78 mcd the range in $\varepsilon_{Nd(0)}$ values appears to narrow ($\Delta\varepsilon_{Nd}$ = 1), though it is important to note that the entire time represented is only ~5 Ma (50–45 Ma) for the H_2O_2-treated material (Table 1). Three replicate samples, from intervals 256.61 mcd, 260.81 mcd, and 275.83 mcd (Table 1), reproduce within analytical error for the H_2O_2-treated material. $\varepsilon_{Nd(0)}$ of (H_2O_2) leached organic coatings from 3 samples (Table 1) yielded values of −7.0, −7.7, and −7.4. These data (unlike for the Sr leachate data) overlap the $\varepsilon_{Nd(0)}$ range for the cleaned (residual) ichthyolith material (Table 1 and Figure 4b). Interestingly, while the paired residue/H_2O_2-leach $\varepsilon_{Nd(0)}$ values are all the same within analytical error (Table 1), two H_2O_2-leachate values (representing leaching experiments performed on different mixtures of the same fish debris in interval 256.61 mcd) yielded $\varepsilon_{Nd(0)}$ slightly outside of analytical error, suggesting slight isotopic heterogeneity in the Nd of the organic coatings (Table 1). Regardless, the overlap in $\varepsilon_{Nd(0)}$ between H_2O_2 leachates and cleaned ichthyolith material (Table 1) is significant, because leachate data generated by a different method (see Methods and Table 2) indicate that a similar range of $\varepsilon_{Nd(0)}$ compositions (−6.4 to −7.0) can be extended down to depth interval 369.59 mcd (~54 Ma) in the ACEX composite record.

[18] The $^{143}Nd/^{144}Nd$ ratios reported here are uncorrected for depositional age (i.e., uncorrected for radiogenic ingrowth). In employing $\varepsilon_{Nd(0)}$ as proxy values for original compositions, we assume that they were closed to Sm/Nd disturbance, evolving along very similar Sm-Nd isotopic paths with constant $^{147}Sm/^{144}Nd$ parent-daughter ratios that are typical of marine biogenic phosphate. To test this assumption, Sm/Nd ratios in a small subset of samples representing leach (H_2O_2) and residue compositions were analyzed by ICP-MS (Table 1), yielding the expected small range in observed $^{147}Sm/^{144}Nd$ (<7% difference in parent/daughter ratio between samples). If the samples are age corrected for initial $^{143}Nd/^{144}Nd$ values at 50 Ma using these parent-daughter ratios, all ε_{Nd} would shift in the positive direction by ~0.35 epsilon units, resulting in a total range in initial ε_{Nd} (50 Ma) of −5.5 to −7.5 (versus −5.8 to −7.8 present day), but still with a $\Delta\varepsilon_{Nd}$ (delta epsilon) of 2. In other words, the ~7% uncertainty in Sm/Nd ratios estimated from these data translates to a < ± 0.07 uncertainty in age-corrected ε_{Nd} (50 Ma) between samples, which is much smaller than analytical error (±0.25 ε_{Nd}); by extrapolation, parallel evolution paths of radiogenic ingrowth can therefore be assumed. Here, we choose to report the Nd isotopic data as the present-day (measured) values (Tables 1 and 2), although the initial value ($\varepsilon_{Nd(50\ Ma)}$) can be obtained by adding ~0.3 + $\varepsilon_{Nd(0)}$.

8. Discussion

8.1. Constraining the History of the Eocene Arctic Ocean From Sr Isotopes

[19] Figure 5 shows the $^{87}Sr/^{86}Sr$ data for early and middle Eocene ACEX fish debris plotted against age, using the time scale of *Backman et al.* [2008]. Intervals of note include the PETM (~55 Ma), the *Azolla* "event" (~48.7 Ma), and the first appearance of ice-rafted debris in the ACEX record at ~46 Ma [*Moran et al.*, 2006; *St. John*, 2008]. Low-salinity events, recorded in the ichthyolith oxygen isotope record assembled by *Waddell and Moore* [2008], show drops in salinity in the Arctic Ocean at Lomonosov Ridge during the PETM, the *Azolla* event, and another salinity drop at ~47.6 Ma (Figure 5). Although the $^{87}Sr/^{86}Sr$ values recorded by fish debris are consistently more radiogenic than Eocene seawater between 55 and 45 Ma (Figure 5), there is no indication that they are shifted toward unusual values (e.g., highly radiogenic) during the low-salinity events (Figure 5).

[20] *Magavern et al.* [1996] reported Sr isotopic results for Eocene fish debris (at ~45 Ma) from a piston core at Alpha Ridge in the Amerasian Basin that are very similar to ours ($^{87}Sr/^{86}Sr$ = 0.7081–0.7086 versus 0.7078–0.7088). They concluded that the high $^{87}Sr/^{86}Sr$ ratios reflected diagenetic alteration and/or Sr gain from surrounding pore waters (cleaning and leaching experiments were not performed in that study). If the Sr isotopic compositions reported here are representative of the upper part of the early middle Eocene water column (i.e., photic zone above the halocline) that existed during the lifetime of these fish species, then periodic influx of large volumes of fresh water to the basin may well be the overall controlling factor on the observed Sr isotopic compositions [*Gleason et al.*, 2007]. However, the age resolution of our data set may also not be adequate to register the effects of specific short-duration events. We repeat here the observation that the variation of Sr isotopic values for the precleaned fish debris does not appear to follow any systematic pattern with age for the

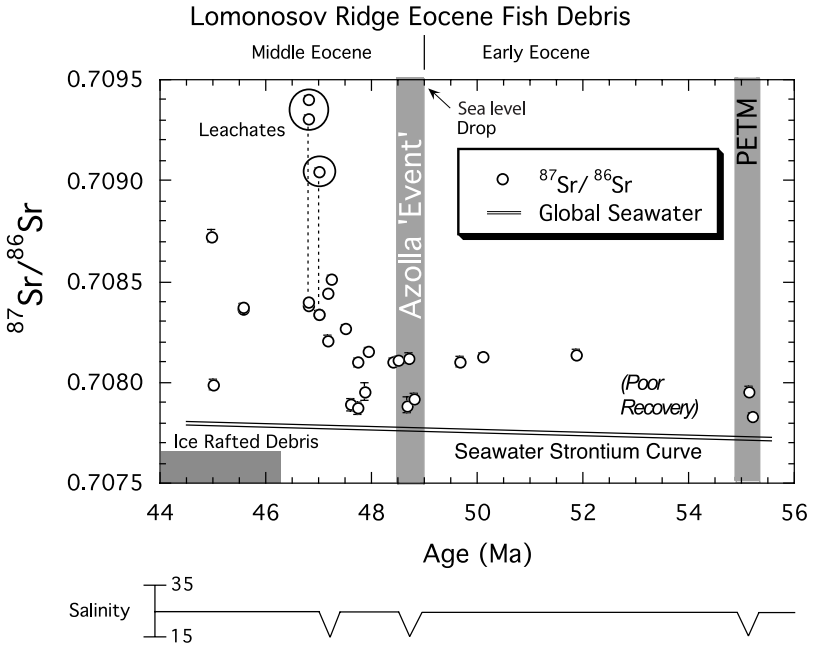

Figure 5. Measured $^{87}Sr/^{86}Sr$ plotted versus age for all cleaned fish debris (residue) material and H_2O_2 leachates analyzed in this study (Table 1). Leachate Sr (see text) is consistently more radiogenic than the cleaned phosphatic fish debris residue (see Figure 4). All the $^{87}Sr/^{86}Sr$ compositions are radiogenic compared to early and middle Eocene seawater Sr [*McArthur et al.*, 2001; *Hodell et al.*, 2007]. Eocene Arctic salinity estimates are approximations from the oxygen isotope salinity study performed by *Waddell and Moore* [2008] on the same fish debris as this study, indicating significant salinity drops at 55 Ma (PETM), 48.6 Ma (*Azolla* event), and an unnamed interval at 47.6 Ma. The $^{87}Sr/^{86}Sr$ variation does not show specific response to these salinity drops but demonstrates overall low-salinity conditions during the ~10 Ma interval studied here (see text).

early to middle Eocene part of the section, with the possible exception of a slight increase toward more radiogenic compositions in younger intervals (Figure 5). A suggestion of greater scatter in the post-46 Ma record, coincident with first appearance of sea ice in the Eocene Arctic Ocean (Figure 5), may be significant but cannot be adequately addressed with this small sample set. Short-term low-salinity events lasting tens to hundreds of thousands of years, such as those that might correspond to thermal spikes in Arctic sea surface temperatures (e.g., during the PETM and early Eocene [*Sluijs et al.*, 2008a, 2008b]) or productivity spikes (e.g., massive blooms of *Azolla* between 49 and 48.3 Ma [*Brinkhuis et al.*, 2006]), may only be resolvable in the Sr isotope record by limiting analyses to material representative of specific individual fish (e.g., single bone, scale or tooth fragments). It is important to note that our Sr isotopic data were obtained from bulk splits of fish debris, and therefore do not reflect the Sr acquired over the lifetime (and therefore the $^{87}Sr/^{86}Sr$) of just one individual fish.

[21] Several lines of evidence suggest that the fish debris we analyzed are representative of the seawater $^{87}Sr/^{86}Sr$ environment within which the host fish dwelt, and are therefore reliable proxies for the salinity environment. The reproducibility of $^{87}Sr/^{86}Sr$ ratios in the cleaned ichthyolith material, i.e., in material obtained from separate fractions of the same interval, highlights the effectiveness of the cleaning process and the "representativeness" of the fractions analyzed. Furthermore, the leaching experiments we performed show the importance of removing the highly radiogenic organic carbon-rich coatings on the ichthyoliths, revealing the cleaned ichthyoliths to have uniformly lower (and more seawater-like) $^{87}Sr/^{86}Sr$ values (Figure 5). Diagenetic alteration and pore water exchange [e.g., *Labs-Hochstein and MacFadden*, 2006] could have affected the ichthyolith $^{87}Sr/^{86}Sr$ ratios, but we consider this to be unlikely. ACEX pore water concentrations [*Expedition 302 Scientists*, 2006] are typically in the range of modern seawater (~80 μM), similar to pore waters in modern Pacific red clays, which impart little or no diagenetic overprint upon associated fish teeth [*Gleason et al.*, 2002, 2004]. Comparisons with the Nd isotopic record (see below) also suggest that diagenetic alteration did not impact the $^{87}Sr/^{86}Sr$ ratios of the cleaned ichthyoliths. We therefore interpret the Sr environment with which the fish equilibrated to have been a low-salinity environment reflective of the measured $^{87}Sr/^{86}Sr$ ratios. If this is a valid assumption, then some independent constraints can be placed on salinity estimates for the Eocene Arctic Ocean using Sr isotopes [e.g., *Ingram and DePaolo*, 1993].

8.2. Eocene Arctic Ocean Salinity Estimates From the Sr Isotope Record

[22] *Waddell and Moore* [2008] reconstructed the early and middle Eocene (55–45 Ma) salinity history of the

Arctic Ocean from $\delta^{18}O_{CO3}$ measurements in the same ichthyolith material that we analyzed for Nd-Sr isotopes. *Waddell and Moore* [2008] calculated average salinities of ~25‰ for the early and middle Eocene Arctic Ocean at Lomonosov Ridge (Figure 5), with three exceptions. They calculated a significant salinity drop at the 55 Ma PETM (to ~17–24‰), although extreme warmth [*Sluijs et al.*, 2006] may account for some of the negative excursion recorded in the ichthyolith $\delta^{18}O_{CO3}$ during this time [*Waddell and Moore*, 2008]. However, low salinities at the Arctic PETM are consistent with other evidence for an accelerated hydrologic cycle, including an expected increase in regional precipitation and runoff associated with extreme high-latitude warmth during the early Eocene climate optimum [*Sluijs et al.*, 2006, 2008a, 2008b; *Pagani et al.*, 2006]. The extent of freshening in the Arctic at the PETM is probably not fully recorded in the reconstruction from oxygen isotopes, because the samples examined were not from the same interval in which *Pagani et al.* [2006] record their highest δD values [*Waddell and Moore*, 2008]. Independent salinity estimates of Arctic surface water at the PETM (IODP Hole 302-4A; unit 3) from deuterium analysis range from 14 to 30‰ [*Pagani et al.*, 2006, Figure 2]. This particular interval is also characterized by an abundance of low-salinity-tolerant dinocysts in the ACEX core [*Sluijs et al.*, 2006], suggesting proximity to riverine sources that probably varied as a function of temperature/eustatic induced transgression/regression sea level cycles [*Sluijs et al.*, 2008a, 2008b]. Thus, surface waters are likely to have remained brackish over the duration of the PETM (although see *Sluijs et al.* [2008a]), consistent with the Sr isotopic data reported here. The two Sr isotopic analyses acquired on fish debris from this interval (Figure 5) establish that Arctic surface water Sr was more radiogenic during the PETM than global seawater, consistent with brackish to fresh water surface conditions at this time (55 Ma). The $^{87}Sr/^{86}Sr$ ratio therefore requires a significant freshwater Sr flux to balance the system (see mixing calculations in Figure 6 and auxiliary material).[1] The surface salinity calculated from the average $^{87}Sr/^{86}Sr$ at the PETM (0.7079) corresponds to a model salinity value of ~6‰.

[23] The lowest salinities obtained by *Waddell and Moore* [2008] from the post-PETM fish debris $\delta^{18}O_{CO3}$ record correspond to events at ~48.7 Ma (i.e., the *Azolla* event [*Brinkhuis et al.*, 2006]), and a previously unidentified low-salinity event at ~47.6 Ma. Both of these shifts in the oxygen isotope record probably correspond to sea level drops of 20–30 m [*Miller et al.*, 2005a], and occurred after connections to Tethys, through the Turgay Strait, had likely ceased at ~49 Ma (Figure 2). The $\delta^{18}O_{CO3}$ salinity range of 16–21‰ calculated for the *Azolla* event [*Waddell and Moore*, 2008] probably does not directly reflect the extremely low salinity (≈fresh water) environment required to support the growth of *Azolla* in open waters [*Brinkhuis et al.*, 2006; *Waddell and Moore*, 2008]; however, the bone carbonate analyzed for O isotopes may have undergone transformations at the sediment-water interface at a depth of a few hundred meters, where salinities were likely much higher within or below the halocline [*Waddell and Moore*, 2008; *Onodera et al.*, 2008; *Stickley et al.*, 2008]. Therefore, the salinities obtained in this way may not reflect the full extent of freshening in surface waters [*Waddell and Moore*, 2008]. The Sr isotopic data are consistent with the oxygen isotope salinity estimates of *Waddell and Moore* [2008], assuming those estimates reflect an upper limit for surface water salinity. *Azolla* (floating fern) tolerates salinities up to 5.5‰ in the laboratory, but its natural tolerance could be even lower (1.0–1.6‰ [*Brinkhuis et al.*, 2006]). The Arctic *Azolla* event (49.0–48.3 Ma), registered in IODP Hole 302-4A (unit 2 of *Moran et al.* [2006]), was a massive event that correlates with regional distribution of *Azolla* as far away as the North Sea [*Brinkhuis et al.*, 2006]. High TOC (~5%) and high primary bioproductivity [*Brinkhuis et al.*, 2006; *Stein et al.*, 2006; *Weller and Stein*, 2008] recorded within this interval are consistent with a high relative influx of fresh water to the Arctic basin during this time [*Brinkhuis et al.*, 2006]. While the Sr isotopic values recorded during this interval may reflect only average isotopic values of surface Sr over thousands to tens of thousands of years, mixing calculations (see Figure 6) using Sr isotopic compositions allow a rough approximation of the freshwater flux to the Eocene Arctic basin to be made. Assuming reasonable compositions for Arctic rivers as part of a two-component mixing equation, average Arctic surface salinities of 2–14‰ during the early and middle Eocene are suggested by the $^{87}Sr/^{86}Sr$ ratios in fish debris (Figure 6). The model (surface water) salinity calculated in this way for the *Azolla* interval (average $^{87}Sr/^{86}Sr = 0.7080$) is ~3‰.

[24] The Sr isotopic data are consistent with multiple lines of evidence indicating strong salinity stratification of the Arctic Ocean over the ~10 Ma duration of the record studied here [*Sluijs et al.*, 2006; *Brinkhuis et al.*, 2006; *Stein et al.*, 2006; *Waddell and Moore*, 2008; *Onodera et al.*, 2008; *Stickley et al.*, 2008]. Long-term stability of a stratified water column must have been maintained even while the evolving tectonic configuration of the basin changed the available exchange routes between the Eocene Arctic and surrounding oceans, concurrent with large oscillations in sea level that caused intermittent cutoff of exchange with the world ocean [*Miller et al.*, 2005a; *Sluijs et al.*, 2008b]. While the dynamic hydrologic cycle of the Eocene Arctic had a significant influence on Eocene Arctic paleoceanography [*Pagani et al.*, 2006; *Sluijs et al.*, 2008a; *Brinkhuis et al.*, 2006], links to the world ocean were nonetheless probably maintained, even if intermittent and shallow, and thus important during this time [*Onodera et al.*, 2008; *Stickley et al.*, 2008]. The $^{87}Sr/^{86}Sr$ variations are best explained by some combination of changes in the balance of river inputs of Sr to the Eocene Arctic Ocean, coupled with oscillation of the halocline above Lomonosov Ridge, and intermittent exchange with surrounding oceans.

8.3. Constraining the History of the Eocene Arctic Ocean From Nd Isotopes

[25] $^{143}Nd/^{144}Nd$ ratios measured in early middle Eocene fish debris at Lomonosov Ridge provide a paleoceanographic

[1] Auxiliary material data sets are available at ftp://ftp.agu.org/apend/pa/2008pa001685. Other auxiliary material files are in the HTML.

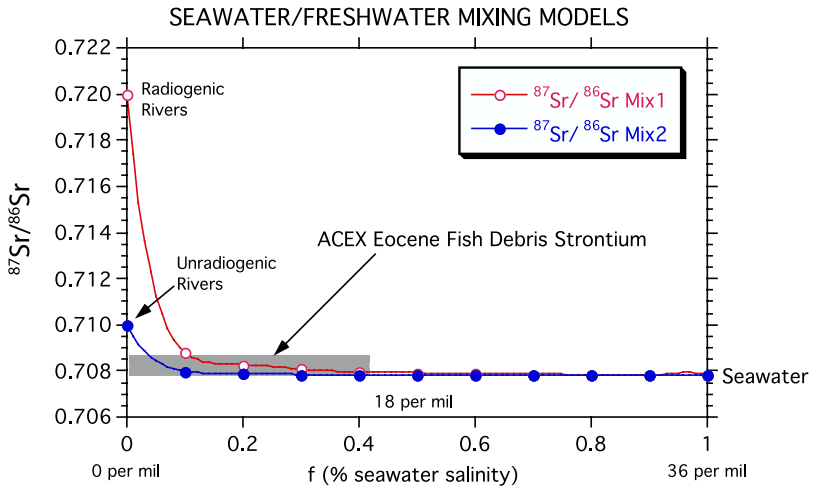

Figure 6. Calculated Sr isotopic mixing curves using (1) radiogenic ($^{87}Sr/^{86}Sr$ = 0.720) and unradiogenic ($^{87}Sr/^{86}Sr$ = 0.710) Arctic river water end-members and (2) early Eocene seawater ($^{87}Sr/^{86}Sr$ = 0.7077). The value for modern Siberian rivers ($^{87}Sr/^{86}Sr$ = 0.7100) incorporates a value for the mean weighted Sr flux [*Huh et al.*, 1998a, 1998b; *Huh and Edmond*, 1999] and is assumed to approximate the most likely fresh water input value to the Eocene Arctic Ocean. Using these input parameters and the data from Table 1, average Eocene Arctic surface water paleosalinities of 2–14‰ (seawater equals ~36‰) are estimated. Paleosalinity values calculated from O isotopes on the same material are 14–24‰ for the Eocene (versus 35‰ for the Miocene Arctic Ocean) but may overestimate surface water salinity for the Eocene Arctic Ocean and are thus an upper limit [*Waddell and Moore*, 2008]. The O isotope-based paleosalinity estimates probably reflect integration and exchange over a deeper water column than the surface water estimates based on Sr data alone. Whole ocean steady state models (see auxiliary materials) for Arctic freshwater Sr flux result in improbable $^{87}Sr/^{86}Sr$ ratios when balanced against hydrothermal and seawater inputs, arguing for a strontium-stratified/salinity-stratified Arctic Ocean between ~55 and ~45 Ma.

"snapshot" of Arctic intermediate water (AIW) flowing across the seafloor at Lomonosov Ridge between 50 Ma and 45 Ma (Table 1 and Figure 7). Because biogenic marine phosphates acquire their REE signal at the sediment-water interface [e.g., *Shaw and Wasserburg*, 1985], and not during the lifetime of the organism, the measured $\varepsilon_{Nd(0)}$ values (~−6 to ~−8) are our best estimate for the Nd isotopic composition of Eocene AIW at ~250–600 m paleodepth [*Moore and Expedition 302 Scientists*, 2006]. Early and middle Eocene AIW at Lomonosov Ridge formed in a high-salinity, oxygen depleted environment below the halocline/thermocline [*Onodera et al.*, 2008; *Stickley et al.*, 2008; *Stein et al.*, 2006; *Waddell and Moore*, 2008], and therefore must have contained a significant component of Nd derived through periodic influx from surrounding ocean basins, as well as from other sources.

[26] Several possible sources of Nd to Eocene AIW at Lomonosov Ridge include (1) open marine inputs, (2) local or regional fluvial/weathering inputs, including boundary exchange processes involving continental margin sediments [*Lacan and Jeandel*, 2005], and (3) remobilized Nd from local diagenetic exchange with pore waters. We rule out the third possibility (diagenetic exchange after burial) as the source of Nd to the fish debris for several reasons. The most likely source of diagenetic Nd that might be incorporated into fish debris during later (burial) diagenesis is the silicate fraction within the sedimentary sequence. However, the Sr and Nd composition of the fish debris remain fully "decoupled" throughout the study interval (Figure 7); that is, samples that record more radiogenic Sr do not record the corresponding unradiogenic Nd values that would indicate a shared continental provenance for both elements (e.g., from silicate exchange with pore waters). The diagenetic potential of Sr in biogenic apatite is greater than that of the trivalent REEs [e.g., *Bertram and Elderfield*, 1993; *Martin and Scher*, 2004], thus any diagenetic alteration of the original Nd isotopic signal acquired at the seawater-sediment interface should be accompanied by overprinting of the primary Sr signal as well, and register as a corresponding shift in both isotopic systems. Since this is not observed (Figure 7), we interpret the fish debris Nd radiogenic isotopic values as primary signatures, and proceed with evaluation of possibilities 1 and 2.

[27] Several lines of evidence indicate that the paleo-Arctic Ocean at Lomonosov Ridge during the early and middle Eocene was strongly stratified, with low-salinity, high-productivity waters dominating the surface environment, and anoxic/euxinic conditions dominating at depth [e.g., *Moran et al.*, 2006; *Brinkhuis et al.*, 2006; *Pagani et al.*, 2006; *Waddell and Moore*, 2008; *Stickley et al.*, 2008; *Onodera et al.*, 2008; *Sluijs et al.*, 2008a; *Weller and Stein*, 2008; *Spofforth et al.*, 2008]. High rates of primary productivity and sediment delivery via rivers could have led to high rates of scavenging of particle reactive dissolved metals [*Sholkovitz*, 1993]. These conditions might then tend to favor local fluvial/weathering inputs as the dominant

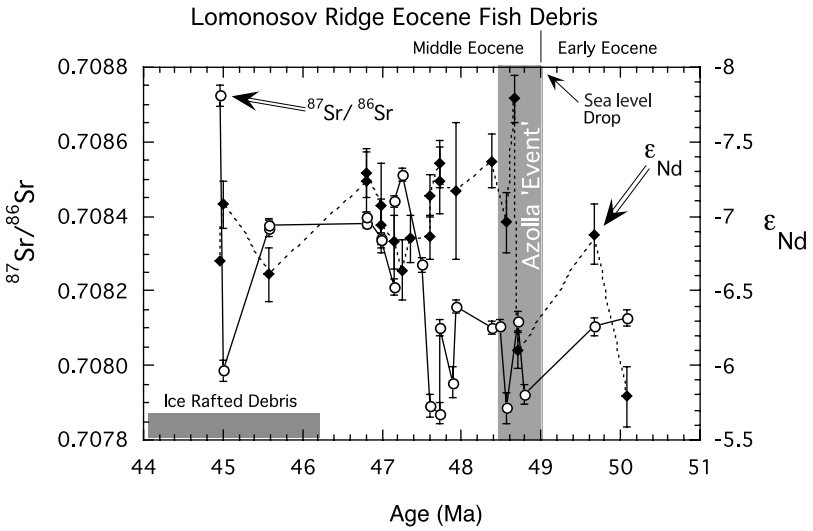

Figure 7. Measured $^{87}Sr/^{86}Sr$ and $^{143}Nd/^{144}Nd$ from Table 1 plotted versus age for a ~5 Ma interval spanning the early and middle Eocene. These data represent the H_2O_2-cleaned fish debris (residue) values only. Here $^{87}Sr/^{86}Sr$ and $\varepsilon_{Nd(0)}$ show no covariance, appearing instead to track separate sources for Sr and Nd (see text).

source of Nd to the waters at the seafloor (that is, direct transport of the surface water Nd signal to the seafloor via particle scavenging [*Grandjean and Albaréde*, 1989]). This scenario would be restricted to transport of the surface water Nd signal to subhalocline depths, without any significant subduction or downwelling in the region, because active advection would be also expected to ventilate the subhalocline waters of the Eocene Arctic Ocean. Rapid mixing, or turnover, and efficient ventilation is inconsistent with (1) the evidence for highly reducing conditions recorded in the sediments and (2) evidence for low-salinity conditions at the surface [*Moran et al.*, 2006; *Stein et al.*, 2006; *Brinkhuis et al.*, 2006; *Spofforth et al.*, 2008; *Waddell and Moore*, 2008]. Boundary exchange processes, involving large-scale remobilization of Nd into the water column from locally derived sediments deposited at basin margins, can be enhanced by anoxic conditions developed within shallow ocean basins [*Lacan and Jeandel*, 2005]. This process has been invoked to explain aspects of the vertical and lateral structure in Nd concentrations and isotopic compositions observed in the oceans, including the modern Arctic [*Arsouze et al.*, 2007; *Porcelli et al.*, 2009], but is difficult to evaluate for a single site within the Eocene Arctic Basin.

[28] While such scavenging mechanisms could explain how fluvial inputs of Nd might have dominated the subhalocline inventory of dissolved Nd in a highly stratified and restricted basin setting, it still does not enable us to reconcile the seemingly decoupled sources of Sr and Nd in the fish debris (Figure 7). While it may be possible to rationalize an Arctic fluvial delivery system that obtained its dissolved Sr inventory from one type of source and its dissolved Nd from another, we are nonetheless left with the likelihood that the Sr and Nd in the fish debris had two different sources/input mechanisms. The Sr source had to be dominantly fluvial, because the fish debris values are consistently and significantly higher than the typical Eocene seawater (Figure 5), and because of the requirement that the Sr in the fish debris was incorporated metabolically from the waters in which the fish dwelt. This means that the most likely source of Nd to the subhalocline waters in the paleo-Arctic basin was, in contrast to Sr, a dominantly marine input.

8.4. Origin of Eocene Arctic Intermediate Water From the Nd Isotope Record

[29] Connections to other marine basins (Figure 2), whether shallow or at intermediate water depths, would have introduced highly saline, and hence denser, waters into the Eocene Arctic basin, as occurs today in the modern Arctic [e.g., *Jakobsson et al.*, 2007]. These denser waters would then have formed intermediate waters at depth. This exchange, or injection, of marine waters from surrounding oceans must have been infrequent, otherwise the dissolved oxygen content of Eocene AIW would have remained relatively high, which is not the case [*Spofforth et al.*, 2008]. Rare earth element patterns recorded in the Eocene fish debris reinforce evidence for anoxic conditions [*Gleason et al.*, 2007]. In the case of periodic ventilation of AIW by injection from open marine sources, high surface water productivity and consequent organic buildup in the Eocene Arctic Ocean would be expected to have rapidly consumed dissolved oxygen below the halocline, maintaining the euxinic/anoxic conditions observed at depth [*Stein et al.*, 2006].

[30] The $\varepsilon_{Nd(0)}$ measured for early/middle Eocene Arctic intermediate waters (AIW) at Lomonosov Ridge (~−6 to ~−8) is less negative (i.e., more radiogenic) than AIW (~200–1,500 m water depth) of the modern central Arctic Ocean (~−10.5 [*Haley et al.*, 2008a; *Andersson et al.*, 2008; *Porcelli et al.*, 2009]), which is formed primarily by the circulation of cooled saline North Atlantic surface waters through the Fram Strait via the Greenland-

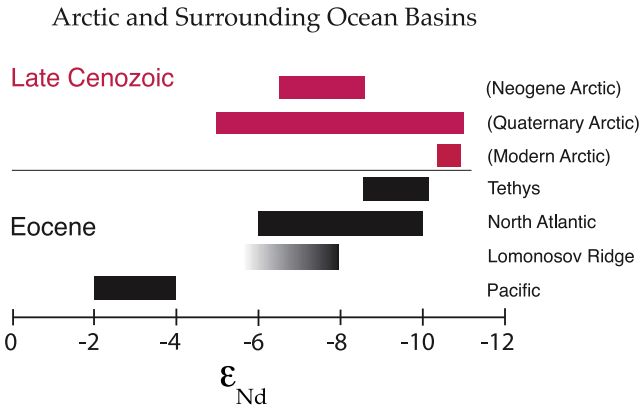

Figure 8. The ε_{Nd} composition ranges of potential marine Nd sources for Eocene Arctic intermediate water at Lomonosov Ridge compared to modern, Quaternary, and Neogene values for the central Arctic Ocean. Nd isotopic compositions are from *Winter et al.* [1997], *Haley et al.* [2008a, 2008b], *Andersson et al.* [2008], *Stille and Fischer* [1990], *Stille et al.* [1996], *Thomas* [2005], *Thomas et al.* [2003], *Porcelli et al.* [2009], and *Zimmermann et al.* [2009]. For comparison, modern Arctic river Nd inputs vary from −5 to −14 [*Porcelli et al.*, 2009].

Norwegian Sea [*Aagaard and Carmack*, 1989; *Jakobsson et al.*, 2007]. ε_{Nd} appears to have varied during the Late Quaternary between unradiogenic (−11) and more radiogenic (−5) values in concert with glacial-interglacial cycles (Figure 8), suggesting the strong influence of ice volume on circulation, sources and transport of water in and around the Arctic Basin [e.g., *Haley et al.*, 2008a, Figure 3]. Best estimates for Neogene (preglacial) AIW are very similar (ε_{Nd} = ∼−6.5 to −8.5) to the Eocene record (Figure 8); however, these radiogenic Neogene values (relative to modern AIW) are currently best explained within the context of sea ice expansion and contraction in the Arctic [*Haley et al.*, 2008a, 2008b], a mechanism that would not have been available before ∼46 Ma for the Arctic Ocean [*Moran et al.*, 2006].

[31] Possible sources of ocean waters available for export and introduction to the Arctic Basin during the Eocene were the Tethys Sea (via the Turgay Strait/western Siberian Seaway), the Pacific Ocean (via a proto-Bering Strait), the Norwegian-Greenland Sea and North Atlantic Ocean (Figure 2). During the early Eocene, Tethys probably had an ε_{Nd} ∼−9 to −10 [*Stille and Fischer*, 1990; *Stille et al.*, 1996], while the North Pacific was more radiogenic (∼−3 [*Thomas*, 2005]). Early Eocene ε_{Nd} values for the Norwegian-Greenland Sea, which may also have been a brackish basin [*Andreasson et al.*, 1996], are not directly constrained but were probably similar to Tethys ε_{Nd} or slightly more radiogenic, given the subaerial exposure of the recently emplaced North Atlantic Igneous Province basalts along the eastern margin of Greenland and western margin of Norway [e.g., *Saunders et al.*, 1997]. The North Atlantic region to the south of (present-day) Iceland had ε_{Nd} (t) values ranging from −5 to −10 during the Eocene [*Thomas et al.*, 2003], bracketing the range of our data set (Figure 8). Given this overlap, it is therefore likely that the variability in the Lomonosov Ridge Eocene ε_{Nd} AIW record reflects changes in the relative contributions of seawater from surrounding ocean basins via (shallow) passageways at that time. Mixing of less radiogenic Nd sources (i.e., Tethys-like) with more radiogenic Nd sources (i.e., Pacific-like) would have been most likely during the early Eocene when connections to Tethys via Turgay Strait were open (Figure 2); however, the overall Nd isotopic signature we obtained for Eocene AIW is most consistent with a North Atlantic dominated Nd flux starting in the early Eocene and extending into the middle Eocene, a possibility that we evaluate in more detail below.

8.5. Origin of Nd Isotopic Variations in the Eocene Arctic Ocean

[32] The relatively wide shift in ε_{Nd} (from ∼−6 to ∼−8) that coincides with the 49–48.3 Ma *Azolla* event in the Arctic (Figure 7) is not duplicated in the $^{87}Sr/^{86}Sr$ ACEX record (Figure 5). This time interval was characterized by lower global sea level, and therefore the potential for effective seawater exchange between the Arctic and surrounding ocean basins should have been extremely limited [*Miller et al.*, 2005b; *Brinkhuis et al.*, 2006; *Waddell and Moore*, 2008]. The fact that ε_{Nd} shifts negative (i.e., less radiogenic) at the *Azolla* low stand event may indicate either an early cutoff or reduction of surface flow from the Pacific (or other radiogenic source), or an enhanced early middle Eocene input from Tethys (via Turgay Strait). The latter is suggested by the sporadic occurrence of highly endemic early middle Eocene siliceous microfossil assemblages common to both the Arctic and western Siberian Sea [*Onodera et al.*, 2008]. However, other workers have concluded that connection with the western Siberian Sea (and Tethys) ended by early middle Eocene time [*Akhmetiev and Beniamovski*, 2004]. The post-*Azolla* middle Eocene Nd record appears to bee less variable (Figure 7), with an average $\varepsilon_{Nd(0)}$ of −7.1 ± 0.5. Intermittent connections to Atlantic and Nordic Seas during the early middle Eocene are supported by siliceous microfossil assemblages that otherwise require strong differences in upper water mass conditions between these regions [*Onodera et al.*, 2008]. The occasional appearance of extremely rare radiolaria in the early middle Eocene ACEX record [*Backman et al.*, 2006] also indicates sporadic connections with open marine waters, though differences in habitat depth among species living above Lomonosov Ridge can probably also explain some of the unusual cooccurrences [*Onodera et al.*, 2008]. Siliceous microfossil assemblages, extremely high sulfur contents and seawater-like S isotopic values at depth [*Onodera et al.*, 2008], indicate more open (and perhaps more frequent) connections to waters of the North Atlantic and/or Nordic Seas after 45 Ma [*Onodera et al.*, 2008] consistent with the Nd isotopic record.

[33] Additional leachate Nd isotope data (Table 2 and Figure 4b) obtained from bulk sediment samples help to extend the ACEX Nd record back to ∼54 Ma, just after the PETM salinity minimum recorded at ∼55 Ma [*Waddell*

and Moore, 2008]. Our data indicate that AIW near the Paleocene/Eocene boundary was similar in its Nd isotopic composition ($\varepsilon_{Nd(0)} = -6.9$, n = 2 (Table 2)) to water circulating above the seafloor at Lomonosov Ridge during the middle Eocene (average $\varepsilon_{Nd(0)}$ of -7.1), including during the *Azolla* fresh water event when sea level was considerably lower, and connections to surrounding oceans more limited [*Brinkhuis et al.*, 2006]. Although the true water depth of the Arctic Ocean above Lomonosov Ridge is essentially unknown at 54–55 Ma [*Moore and Expedition 302 Scientists*, 2006], and Arctic connections to the world ocean poorly documented near the Paleocene/Eocene boundary [see *Sluijs et al.*, 2006, Figure 1], a eustatic sea level rise is indicated at the PETM [*Sluijs et al.*, 2008b] when euxinic conditions in the Arctic Ocean were already established, requiring that a stratified water column had evolved by ~1 Ma after marine sedimentation commenced at Lomonosov Ridge at around 56 Ma [*Backman et al.*, 2006; *Stein et al.*, 2006; *Sluijs et al.*, 2008b]. The establishment of a semipermanent fresh water to brackish lens at the surface of the paleo-Arctic Ocean was probably catalyzed by an extremely dynamic Arctic hydrologic cycle during the PETM [*Pagani et al.*, 2006], while bottom waters continued to be periodically replenished through input from some combination of Pacific Ocean (as seen today in the Canada Basin [*Porcelli et al.*, 2009]), North Atlantic/Norwegian-Greenland Sea, and Tethys Sea as sources for Nd. The fact that the Nd isotopic signal appears to be fairly constant over the ~10 Ma time interval studied suggests that the relative proportions of these sources did not change dramatically. Although a North Atlantic source of Nd is likely to have been an important component of this mix through the middle Eocene, we hypothesize that Tethyan and Pacific sources also contributed to the Nd signature of AIW during the early Eocene, and possibly into the middle Eocene as well. Without the identification of more extreme radiogenic end-member compositions in the Eocene ACEX record (e.g., > -6 or < -8), however, we must conclude that the relatively narrow range of ε_{Nd} reflects a mixed signature consistent with roughly proportional contributions from multiple marine sources to AIW at Lomonosov Ridge between ~55 Ma and ~45 Ma.

9. Conclusions

[34] ε_{Nd} compositions measured in early to middle Eocene ichthyoliths from Lomonosov Ridge (IODP Arctic Coring Expedition 302) are distinctly more radiogenic than modern Arctic intermediate water (AIW), suggesting several possible sources of Nd to the Eocene Arctic Ocean. Marine inputs from the Tethys Sea (via the Turgay Strait/western Siberian Seaway), Pacific Ocean (via a proto-Bering Strait) and Norwegian-Greenland Sea/North Atlantic Ocean were all likely important, though intermittent, sources of the AIW Nd signature at Lomonosov Ridge between 55 and 45 Ma. The Eocene Sr isotopic record, in contrast, is very consistent with fresh to brackish surface water conditions persisting for ~10 million years at this location. Fresh water inputs at the surface via direct precipitation and rivers, combined with unprecedented early and middle Eocene warmth, supported a dynamic Arctic hydrologic cycle that, combined with eustatic-tectonic controls on oceanic exchange, helped maintain a strongly salinity-stratified water column in the paleo-Arctic Ocean.

[35] **Acknowledgments.** This research was supported by NSF grant OCE-0550702 awarded to the University of Michigan and Texas A&M University and by the Integrated Ocean Drilling Program. L. Waddell is thanked for her collaborative efforts on our behalf and for the photography used in Figure 3. M. Johnson, C. Henderson, T. Huston, and J. Reuss all provided laboratory technical assistance at various stages of this project. D. Austin helped with drafting of figures. E. Martin and an anonymous reviewer provided especially helpful and constructive comments for improving the manuscript.

References

Aagaard, K., and E. C. Carmack (1989), The role of sea ice and other fresh water in the Arctic circulation, *J. Geophys. Res.*, *94*, 14,485–14,498, doi:10.1029/JC094iC10p14485.

Aagaard, K., and E. C. Carmack (1994), The Arctic Ocean and climate: A perspective, in *The Polar Oceans and Their Role in Shaping the Global Environment: The Nansen Centennial Volume*, *Geophys. Monogr. Ser.*, vol. 85, edited by O. M. Johannessen, R. D. Muench, and J. E. Overland, pp. 5–20, AGU, Washington, D. C.

Akhmetiev, M. A., and V. N. Beniamovski (2004), Paleocene and Eocene of western Europe (Russian sector)—Stratigraphy, palaeogeography, and climate, *Neues Jahrb. Geol. Palaeontol. Abh.*, *234*, 137–181.

Amakawa, H., D. S. Alibo, and Y. Nozaki (2000), Nd isotopic composition and REE pattern in the surface waters of the eastern Indian Ocean and its adjacent seas, *Geochim. Cosmochim. Acta*, *64*, 1715–1727, doi:10.1016/S0016-7037(00)00333-1.

Andersson, P. S., D. Porcelli, M. Frank, G. Björk, R. Dahlqvst, and Ö. Gustafsson (2008), Neodymium isotopes in seawater from the Barents Sea and Fram Strait Arctic-Atlantic gateways, *Geochim. Cosmochim. Acta*, *72*, 2854–2867, doi:10.1016/j.gca.2008.04.008.

Andreasson, F. P., B. Schmitz, and D. Spiegler (1996), Stable isotopic composition ($\delta^{18}O_{CO3}$, $\delta^{13}C$) of early Eocene fish-apatite from Hole 913B: An indicator of the early Norwegian–Greenland Sea paleosalinity, *Proc. Ocean Drill. Program Sci. Results*, *151*, 583–591.

Arsouze, T., J.-C. Dutay, F. Lacan, and C. Jeandel (2007), Modeling the neodymium isotopic composition with a global ocean circulation model, *Chem. Geol.*, *239*, 165–177, doi:10.1016/j.chemgeo.2006.12.006.

Backman, J., and K. Moran (2008), Introduction to special section on Cenozoic paleoceanography of the central Arctic Ocean, *Paleoceanography*, *23*, PA1S01, doi:10.1029/2007PA001516.

Backman, J., K. Moran, D. B. McInroy, L. A. Mayer, and Expedition Scientists (2006), *Proceedings of the Integrated Ocean Drilling Program*, vol. 302, Integrated Ocean Drill. Program Manage. Int., College Station, Tex.

Backman, J., et al. (2008), Age model and core-seismic integration for the Cenozoic Arctic Coring Expedition sediments from the Lomonosov Ridge, *Paleoceanography*, *23*, PA1S03, doi:10.1029/2007PA001476.

Bertram, C. J., and H. Elderfield (1993), The geochemical balance of the rare earth elements and neodymium isotopes in the oceans, *Geochim. Cosmochim. Acta*, *57*, 1957–1986, doi:10.1016/0016-7037(93)90087-D.

Boyle, E. A. (1981), Cadmium, zinc, copper and barium in foraminifera tests, *Earth Planet. Sci. Lett.*, *53*, 11–35, doi:10.1016/0012-821X(81)90022-4.

Brinkhuis, H., et al. (2006), Episodic fresh surface water in the Eocene Arctic Ocean, *Nature*, *441*, 606–609, doi:10.1038/nature04692.

Broecker, W. S., D. M. Peteet, and D. Rind (1985), Does the ocean-atmosphere system have more than one stable mode of operation?, *Nature*, *315*, 21–26, doi:10.1038/315021a0.

Bukry, D. (1984), Paleogene paleoceanography of the Arctic Ocean is constrained by the middle or late Eocene age of USGS Core Fl-422: Evidence from silicoflagellates, *Geology*, *12*, 199–201, doi:10.1130/0091-7613(1984)12<199:PPOTAO>2.0.CO;2.

Crowley, T. J., and K.-Y. Kim (1995), Comparison of longterm greenhouse projections with the geologic record, *Geophys. Res. Lett.*, *22*, 933–936, doi:10.1029/95GL00799.

Crowley, T. J., and J. C. Zachos (2000), Comparison of zonal temperature profiles for past warm time periods, in *Warm Climates in Earth History*, edited by B. T. Huber, K. S. MacLeod, and S. C. Wing, pp. 425–444, Cambridge Univ. Press, Cambridge, U. K.

Dai, A., T. M. L. Wigley, B. A. Boville, J. T. Kiehl, and L. E. Buja (2001), Climates of the twentieth and twenty-first centuries simulated by the NCAR climate system model, *Bull. Am. Meteorol. Soc.*, *14*, 485–519.

DePaolo, D. J., and G. J. Wasserburg (1976), Nd isotopic variations and petrogenetic models, *Geophys. Res. Lett.*, *3*, 248–252.

Elderfield, H., R. Upstill-Goddard, and E. R. Sholkovitz (1990), The rare earth elements in rivers, estuaries, and coastal seas and their significance to the composition of ocean waters, *Geochim. Cosmochim. Acta*, *54*, 971–991, doi:10.1016/0016-7037(90)90432-K.

Expedition 302 Scientists (2005), Arctic Coring Expedition: Paleoceanographic and tectonic evolution of the central Arctic Ocean, *Prelim. Rep. Integrated Ocean Drill. Program*, *302*, 1–8, doi:10.2204/iodp.pr.302.2005.

Expedition 302 Scientists (2006), Sites M0001–M0004, *Proc. Integrated Ocean Drill. Program*, *302*, 1–169, doi.10.2204/iodp.proc.302.104.2006.

Frank, M. (2002), Radiogenic isotopes: Tracers of past ocean circulation and erosional input, *Rev. Geophys.*, *40*(1), 1001, doi:10.1029/2000RG000094.

Gleason, J. D., T. C. Moore, D. K. Rea, T. M. Johnson, R. M. Owen, J. D. Blum, S. A. Hovan, and C. E. Jones (2002), Ichthyolith strontium isotope stratigraphy of a Neogene red clay sequence: Calibrating eolian dust accumulation rates in the central North Pacific, *Earth Planet. Sci. Lett.*, *202*, 625–636, doi:10.1016/S0012-821X(02)00827-0.

Gleason, J. D., T. C. Moore Jr., T. M. Johnson, D. K. Rea, R. M. Owen, J. D. Blum, J. Pares, and S. A. Hovan (2004), Age calibration of piston core EW9709-07 (equatorial central Pacific) using fish teeth Sr isotope stratigraphy, *Palaeogeogr. Palaeoclimatol. Palaeoecol.*, *212*, 355–366.

Gleason, J. D., D. J. Thomas, T. C. Moore Jr., J. D. Blum, R. M. Owen, and B. A. Haley (2007), Water column structure of the Eocene Arctic Ocean recorded by Nd-Sr isotope proxies in fossil fish debris, *Geochim. Cosmochim. Acta*, *71*, A239.

Goldstein, S. L., and S. R. Hemming (2003), Long-lived isotopic tracers in oceanography, paleoceanography and ice sheet dynamics, in *Treatise on Geochemistry*, vol. 6, *The Oceans and Marine Geochemistry*, edited by H. Elderfield, pp. 453–489, Elsevier, Oxford, U. K.

Goldstein, S. J., and S. B. Jacobsen (1988), Nd and Sr isotopic systematics of river water suspended material: Implications for crustal evolution, *Earth Planet. Sci. Lett.*, *87*, 249–265, doi:10.1016/0012-821X(88)90013-1.

Grandjean, P., and F. Albaréde (1989), Ion probe measurement of rare earth elements in biogenic phosphates, *Geochim. Cosmochim. Acta*, *53*, 3179–3183.

Haley, B. A., M. Frank, R. F. Spielhagen, and A. Eisenhauer (2008a), Influence of brine formation on Arctic Ocean circulation over the past 15 million years, *Nat. Geosci.*, *1*, 68–72, doi:10.1038/ngeo.2007.5.

Haley, B. A., M. Frank, R. F. Spielhagen, and J. Fietzke (2008b), Radiogenic isotope record of Arctic Ocean circulation and weathering inputs of the past 15 million years, *Paleoceanography*, *23*, PA1S13, doi:10.1029/2007PA001486.

Halliday, A. N., J. P. Davidson, P. Holden, R. M. Owen, and A. M. Olivarez (1992), Metalliferous sediments and the scavenging residence time of Nd near hydrothermal vents, *Geophys. Res. Lett.*, *19*, 761–764, doi:10.1029/92GL00393.

Hodell, D. A., G. D. Kamenov, E. C. Hathorne, J. C. Zachos, U. Röhl, and T. Westerhold (2007), Variations in the strontium isotope composition of seawater during the Paleocene and early Eocene from ODP Leg 208 (Walvis Ridge), *Geochem. Geophys. Geosyst.*, *8*, Q09001, doi:10.1029/2007GC001607.

Holmden, C., R. A. Creaser, and K. Muehlenbachs (1997), Paleosalinities in ancient brackish water systems determined by $^{87}Sr/^{86}Sr$ in carbonate fossils: A case study from the Western Canada Sedimentary Basin, *Geochim. Cosmochim. Acta*, *61*, 2105–2118.

Huh, Y., and J. M. Edmond (1999), The fluvial geochemistry of the rivers of Eastern Siberia: III. Tributaries of the Lena and Anabar draining the basement terrain of the Siberian Craton and the Trans-Baikal Highlands, *Geochim. Cosmochim. Acta*, *63*, 967–987, doi:10.1016/S0016-7037(99)00045-9.

Huh, Y., M.-Y. Tsoi, A. Zaitsev, and J. M. Edmond (1998a), The fluvial geochemistry of the rivers of Eastern Siberia: I. Tributaries of the Lena River draining the sedimentary platform of the Siberian Craton, *Geochim. Cosmochim. Acta*, *62*, 1657–1676, doi:10.1016/S0016-7037(98)00107-0.

Huh, Y., G. Panteleyev, D. Babich, A. Zaitsev, and J. M. Edmond (1998b), The fluvial geochemistry of the rivers of eastern Siberia: II. Tributaries of the Lena, Omoloy, Yana, Indigirka, Kolyma, and Anadyr draining the collisional/accretionary zone of the Verkhoyansk and Cherskiy ranges, *Geochim. Cosmochim. Acta*, *62*, 2053–2075, doi:10.1016/S0016-7037(98)00127-6.

Iakovleva, A. I., H. Brinkhuis, and C. Cavagnetto (2001), Late Paleocene–early Eocene dinoflagellate cysts from the Turgay Strait, Kazakhstan: Correlations across ancient seaways, *Palaeogeogr. Palaeoclimatol. Palaeoecol.*, *172*, 243–268, doi:10.1016/S0031-0182(01)00300-5.

Ingram, B. L. (1995), High-resolution dating of deep-sea clays using Sr isotopes in fossil fish teeth, *Earth Planet. Sci. Lett.*, *134*, 545–555, doi:10.1016/0012-821X(95)00151-2.

Ingram, B. L., and D. J. DePaolo (1993), A 4300 year strontium isotope record of estuarine paleosalinity in San Francisco Bay, California, *Earth Planet. Sci. Lett.*, *119*, 103–119, doi:10.1016/0012-821X(93)90009-X.

Jahren, A. H., and L. S. L. Sternberg (2003), Humidity estimate for the middle Eocene Arctic rain forest, *Geology*, *31*, 463–466, doi:10.1130/0091-7613(2003)031<0463:HEFTME>2.0.CO;2.

Jakobsson, M., N. Cherkis, J. Woodward, R. Macnab, and B. Coakley (2000), New grid of Arctic bathymetry aids scientists and mapmakers, *Eos Trans. AGU*, *81*(9), 89.

Jakobsson, M., et al. (2007), The early Miocene onset of a ventilated circulation regime in the Arctic Ocean, *Nature*, *447*, 986–990, doi:10.1038/nature05924.

Jeandel, C. (1993), Concentration and isotopic composition of Nd in the South Atlantic Ocean, *Earth Planet. Sci. Lett.*, *117*, 581–591, doi:10.1016/0012-821X(93)90104-H.

Jeandel, C., T. Arsouze, F. Lacan, P. Téchiné, and J.-C. Dutay (2007), Isotopic Nd compositions and concentrations of the lithogenic inputs into the ocean: A compilation, with emphasis on the margins, *Chem. Geol.*, *239*, 156–164, doi:10.1016/j.chemgeo.2006.11.013.

Johnson, G. L., J. Pogrebitsky, and R. Macnab (1994), Arctic structural evolution: Relationship to paleoceanography, in *The Polar Oceans and Their Role in Shaping the Global Environment: The Nansen Centennial Volume*, *Geophys. Monogr. Ser.*, vol. 85, edited by O. M. Johannessen, R. D. Muench, and J. E. Overland, pp. 285–294, AGU, Washington, D. C.

Knies, J., U. Mann, B. N. Popp, R. Stein, and H.-J. Brumsack (2008), Surface water productivity and paleoceanographic implications in the Cenozoic Arctic Ocean, *Paleoceanography*, *23*, PA1S16, doi:10.1029/2007PA001455.

Labs-Hochstein, J., and B. J. MacFadden (2006), Quantification of diagenesis in Cenozoic sharks: Elemental and mineralogical changes, *Geochim. Cosmochim. Acta*, *70*, 4921–4932.

Lacan, F., and C. Jeandel (2005), Neodymium isotopes as a new tool for quantifying exchange fluxes at the continent-ocean interface, *Earth Planet. Sci. Lett.*, *232*, 245–257, doi:10.1016/j.epsl.2005.01.004.

Lawver, L. A., A. Grantz, and L. M. Gahagan (2002), Plate kinematic evolution of the present Arctic region since the Ordovician, in *Tectonic Evolution of the Bering Shelf–Chuckchi Sea–Arctic Margin and Adjacent Landmasses*, edited by E. L. Miller, A. Grantz, and S. L. Klemperer, *Spec. Pap. Geol. Soc. Am.*, *360*, 333–358.

Magavern, S., D. L. Clark, and S. L. Clark (1996), $^{87/86}Sr$, phytoplankton, and the nature of the Late Cretaceous and Early Cenozoic Arctic Ocean, *Mar. Geol.*, *133*, 183–192, doi:10.1016/0025-3227(96)00024-2.

Marincovich, L., E. M. Brouwers, D. M. Hopkins, and M. C. McKenna (1990), Late Mesozoic and Cenozoic paleogeographic and paleoclimatic history of the Arctic Ocean Basin, based on shallow-water marine faunas and terrestrial vertebrates, in *The Arctic Ocean Region*, edited by A. Grantz, L. Johnson, and J. F. Sweeney, pp. 403–406, Geol. Soc. of Am., Boulder, Colo.

Martin, E. E., and B. A. Haley (2000), Fossil fish teeth as proxies for seawater Sr and Nd isotopes, *Geochim. Cosmochim. Acta*, *64*, 835–847, doi:10.1016/S0016-7037(99)00376-2.

Martin, E. E., and H. D. Scher (2004), Preservation of seawater Sr and Nd isotopes in fossil fish teeth: Bad news and good news, *Earth Planet. Sci. Lett.*, *220*, 25–39, doi:10.1016/S0012-821X(04)00030-5.

McArthur, J. M., R. J. Howarth, and T. R. Bailey (2001), Strontium isotope stratigraphy: LOWESS version 3—Best fit to the marine Sr-isotope curve for 0–509 Ma and accompanying look-up table for deriving numerical age, *J. Geol.*, *109*, 155–170, doi:10.1086/319243.

Meyer, K. M., and L. R. Kump (2008), Oceanic anoxia in Earth history: Causes and consequences, *Annu. Rev. Earth Planet. Sci.*, *36*, 251–288, doi:10.1146/annurev.earth.36.031207.124256.

Miller, K. G., M. A. Kominz, J. V. Browning, J. D. Wright, G. S. Mountain, M. E. Katz, P. J. Sugarman, B. S. Cramer, N. Christie-Blick, and S. F. Pekar (2005a), The Phanerozoic record of global sea-level change, *Science*, *310*, 1293–1298, doi:10.1126/science.1116412.

Miller, K. G., J. D. Wright, and J. V. Browning (2005b), Visions of ice sheets in a greenhouse

world, *Mar. Geol.*, *217*, 215–231, doi:10.1016/j.margeo.2005.02.007.

Moore, T. C. and Expedition 302 Scientists (2006), Sedimentation and subsidence history of the Lomonosov Ridge, *Proc. Integrated Ocean Drill. Program*, *302*, 1–7, doi:10.2204/iodp.proc.302.105.2006.

Moran, K., et al. (2006), The Cenozoic palaeoenvironment of the Arctic Ocean, *Nature*, *441*, 601–605, doi:10.1038/nature04800.

Onodera, J., K. Takahashi, and R. W. Jordan (2008), Eocene silicoflagellate and ebridian paleoceanography in the central Arctic Ocean, *Paleoceanography*, *23*, PA1S15, doi:10.1029/2007PA001474.

O'Regan, M., J. King, J. Backman, M. Jakobsson, H. Pälike, K. Moran, C. Heil, T. Sakamoto, T. M. Cronin, and R. W. Jordan (2008), Constraints on the Pleistocene chronology of sediments from the Lomonosov Ridge, *Paleoceanography*, *23*, PA1S19, doi:10.1029/2007PA001551.

Pagani, M., J. C. Zachos, K. H. Freeman, B. Tipple, and S. Bohaty (2005), Marked decline in atmospheric carbon dioxide concentrations during the Paleogene, *Science*, *309*, 600–603, doi:10.1126/science.1110063.

Pagani, M., et al. (2006), Arctic hydrology during global warming at the Paleocene/Eocene thermal maximum, *Nature*, *442*, 671–675, doi:10.1038/nature05043.

Pälike, H., D. J. A. Spofforth, M. O'Regan, and J. Gattacceca (2008), Orbital scale variations and timescales from the Arctic Ocean, *Paleoceanography*, *23*, PA1S10, doi:10.1029/2007PA001490.

Palmer, M. R., and J. M. Edmond (1989), The strontium isotope budget of the modern ocean, *Earth Planet. Sci. Lett.*, *92*, 11–26, doi:10.1016/0012-821X(89)90017-4.

Pearson, P. N., and M. R. Palmer (2000), Atmospheric carbon dioxide concentrations over the past 60 million years, *Nature*, *406*, 695–699, doi:10.1038/35021000.

Piepgras, D. J., and S. B. Jacobsen (1988), The isotopic composition of neodymium in the North Pacific, *Geochim. Cosmochim. Acta*, *52*, 1373–1381, doi:10.1016/0016-7037(88)90208-6.

Piepgras, D. J., and G. J. Wasserburg (1987), Rare earth element transport in the western North Atlantic inferred from Nd isotopic observations, *Geochim. Cosmochim. Acta*, *51*, 1257–1271, doi:10.1016/0016-7037(87)90217-1.

Porcelli, D., P. S. Andersson, M. Baskaran, M. Frank, G. Björk, and I. Semiletov (2009), The distribution of neodymium isotopes in Arctic Ocean basins, *Geochim. Cosmochim. Acta*, *73*, 2645–2659.

Radionova, E. P., and I. E. Khokhlova (2000), Was the North Atlantic connected with the Tethys via the Arctic in the early Eocene? Evidence from siliceous plankton, *GFF*, *122*, 133–134.

Radionova, E. P., V. N. Beniamovski, A. I. Iakovleva, N. G. Muzylöv, T. V. Oreshkina, E. A. Shcherbinina, and G. E. Kozlova (2003), Early Paleogene transgressions: Stratigraphical and sedimentological evidence from the northern Peri-Tethys, in *Causes and Consequences of Globally Warm Climates in the Early Paleogene*, edited by S. L. Wing et al., *Spec. Pap. Geol. Soc. Am.*, *393*, 239–261.

Reynard, B., C. Lécuyer, and P. Grandjean (1999), Crystal-chemical controls on rare-earth element concentrations in fossil biogenic apatites and implications for paleoenvironmental reconstructions, *Chem. Geol.*, *155*, 233–241, doi:10.1016/S0009-2541(98)00169-7.

Richter, F. M., and K. K. Turekian (1993), Simple models for the geochemical response of the ocean to climatic and tectonic forcing, *Earth Planet. Sci. Lett.*, *119*, 121–131, doi:10.1016/0012-821X(93)90010-7.

Sangiorgi, F., E. E. vanSoelen, D. J. A. Spofforth, H. Pälike, C. E. Stickley, K. St. John, N. Koç, S. Schouten, J. S. SinninghеDamsté, and H. Brinkhuis (2008a), Cyclicity in the middle Eocene central Arctic Ocean sediment record: Orbital forcing and environmental response, *Paleoceanography*, *23*, PA1S08, doi:10.1029/2007PA001487.

Sangiorgi, F., H.-J. Brumsack, D. A. Willard, S. Schouten, C. E. Stickley, M. O'Regan, G.-J. Reichart, J. S. Sinninghe Damsté, and H. Brinkhuis (2008b), A 26 million year gap in the central Arctic record at the greenhouse-icehouse transition: Looking for clues, *Paleoceanography*, *23*, PA1S04, doi:10.1029/2007PA001477.

Saunders, A. D., J. G. Fitton, A. C. Kerr, M. J. Norry, and R. W. Kent (1997), The North Atlantic igneous province, in *Large Igneous Provinces: Continental, Oceanic, and Planetary Flood Volcanism*, *Geophys. Monogr. Ser.*, vol. 100, edited by J. J. Mahoney and M. F. Coffin, pp. 45–93, AGU, Washington, D. C.

Schmitz, B., G. Åberg, L. Werdelin, P. Forey, and S. E. Bendix-Almgreen (1991), $^{87}Sr/^{86}Sr$, Na, F, Sr, and La in skeletal fish debris as a measure of the paleosalinity of fossil-fish habitats, *Geol. Soc. Am. Bull.*, *103*, 786–794, doi:10.1130/0016-7606(1991)103<0786:SSNFSA>2.3.CO;2.

Shaw, H.-F., and G. J. Wasserburg (1985), Sm-Nd in marine carbonates and phosphates: Implications for Nd isotopes in seawater and crustal ages, *Geochim. Cosmochim. Acta*, *49*, 503–518, doi:10.1016/0016-7037(85)90042-0.

Sholkovitz, E. R. (1993), The geochemistry of rare earth elements in the Amazon River estuary, *Geochim. Cosmochim. Acta*, *57*, 2181–2190, doi:10.1016/0016-7037(93)90559-F.

Sloan, L. C., and D. K. Rea (1996), Atmospheric carbon dioxide and early Eocene climate: A general circulation modeling sensitivity study, *Palaeogeogr. Palaeoclimatol. Palaeoecol.*, *119*, 275–292, doi:10.1016/0031-0182(95)00012-7.

Sloan, L. C., J. C. G. Walker, T. C. Moore, D. K. Rea, and J. C. Zachos (1992), Possible methane-induced polar warming in the early Eocene, *Nature*, *357*, 320–322, doi:10.1038/357320a0.

Sluijs, A., et al. (2006), Subtropical Arctic Ocean temperatures during the Paleocene/Eocene thermal maximum, *Nature*, *441*, 610–613, doi:10.1038/nature04668.

Sluijs, A., U. Röhl, S. Schouten, H.-J. Brumsack, F. Sangiorgi, J. S. Sinninghe Damsté, and H. Brinkhuis (2008a), Arctic late Paleocene–early Eocene paleoenvironments with special emphasis on the Paleocene-Eocene thermal maximum (Lomonosov Ridge Integrated Ocean Drilling Program Expedition 302), *Paleoceanography*, *23*, PA1S11, doi:10.1029/2007PA001495.

Sluijs, A., et al. (2008b), Eustatic variations during the Paleocene-Eocene greenhouse world, *Paleoceanography*, *23*, PA4216, doi:10.1029/2008PA001615.

Spofforth, D. J. A., H. Pälike, and D. Green (2008), Paleogene record of elemental concentrations in sediments from the Arctic Ocean obtained by XRF analyses, *Paleoceanography*, *23*, PA1S09, doi:10.1029/2007PA001489.

Staudigel, H., P. Doyle, and A. Zindler (1985), Sr and Nd isotope systematics in fish teeth, *Earth Planet. Sci. Lett.*, *76*, 45–56, doi:10.1016/0012-821X(85)90147-5.

Stein, R., B. Boucsein, and H. Meyer (2006), Anoxia and high primary production in the Paleogene central Arctic Ocean: First detailed records from the Lomonosov Ridge, *Geophys. Res. Lett.*, *33*, L18606, doi:10.1029/2006GL026776.

Stickley, C. E., N. Koç, H.-J. Brumsack, R. W. Jordan, and I. Suto (2008), A siliceous microfossil view of middle Eocene Arctic paleoenvironments: A window of biosilica production and preservation, *Paleoceanography*, *23*, PA1S14, doi:10.1029/2007PA001485.

Stille, P., and H. Fischer (1990), Secular variation in the isotopic composition of Nd in Tethys seawater, *Geochim. Cosmochim. Acta*, *54*, 3139–3145, doi:10.1016/0016-7037(90)90129-9.

Stille, P., M. Steinmann, and S. R. Riggs (1996), Nd isotope evidence for the evolution of paleocurrents in the Atlantic and Tethys oceans during the past 180 Myr, *Earth Planet. Sci. Lett.*, *144*, 9–19, doi:10.1016/0012-821X(96)00157-4.

St. John, K. (2008), Cenozoic ice-rafting history of the central Arctic Ocean: Terrigenous sands on the Lomonosov Ridge, *Paleoceanography*, *23*, PA1S05, doi:10.1029/2007PA001483.

Tachikawa, K., C. Jeandel, and M. Roy-Barman (1999), A new approach to the Nd residence time in the ocean: The role of atmospheric inputs, *Earth Planet. Sci. Lett.*, *170*, 433–446, doi:10.1016/S0012-821X(99)00127-2.

Tanaka, T., et al. (2000), JNdi-1: A neodymium isotopic reference in consistency with LaJolla neodymium, *Chem. Geol.*, *168*, 279–281, doi:10.1016/S0009-2541(00)00198-4.

Thiede, J., and A. M. Myhre (1996), Introduction to the North Atlantic–Arctic gateways: Plate tectonic-paleoceanographic history and significance, *Proc. Ocean Drill. Program Sci. Results*, *151*, 3–23.

Thomas, D. J. (2005), Reconstructing ancient deep-sea circulation patterns using the Nd isotopic composition of fossil fish debris, in *Isotopic and Elemental Tracers of Cenozoic Climate Change*, edited by G. Mora and D. Surge, *Spec. Pap. Geol. Soc. Am.*, *395*, 1–12.

Thomas, D. J., and R. K. Via (2007), Neogene evolution of Atlantic thermohaline circulation: Perspective from Walvis Ridge, southeastern Atlantic Ocean, *Paleoceanography*, *22*, PA2212, doi:10.1029/2006PA001297.

Thomas, D. J., T. J. Bralower, and C. E. Jones (2003), Neodymium isotopic reconstruction of late Paleocene–early Eocene thermohaline circulation, *Earth Planet. Sci. Lett.*, *209*, 309–322, doi:10.1016/S0012-821X(03)00096-7.

Waddell, L. M., and T. C. Moore (2008), Salinity of the Eocene Arctic Ocean from oxygen isotope analysis of fish bone carbonate, *Paleoceanography*, *23*, PA1S12, doi:10.1029/2007PA001451.

Weijers, J. W. H., S. Schouten, A. Sluijs, H. Brinkhuis, and J. S. Sinninghe Damsté (2007), Warm Arctic continents during the Palaeocene-Eocene thermal maximum, *Earth Planet. Sci. Lett.*, *261*, 230–238, doi:10.1016/j.epsl.2007.06.033.

Weller, P., and R. Stein (2008), Paleogene biomarker records from the central Arctic Ocean (Integrated Ocean Drilling Program Expedition 302): Organic carbon sources, anoxia, and sea surface temperatures, *Paleoceanography*, *23*, PA1S17, doi:10.1029/2007PA001472.

Winter, B. L., C. M. Johnson, and D. L. Clark (1997), Strontium, neodymium, and lead isotope variations of authigenic and silicate sediment components from the Late Cenozoic Arctic Ocean: Implications for sediment provenance and the source of trace metals in seawater, *Geochim. Cosmochim. Acta*, *61*, 4181–4200, doi:10.1016/S0016-7037(97)00215-9.

Wright, J., R. S. Seymour, and H. Shaw (1984), REE and Nd isotopes in conodont apatite: Variations with geological age and depositional environment, in *Conodont Biofacies and Provincialism*, edited by D. L. Clark, *Spec. Pap. Geol. Soc. Am.*, *196*, 325–340.

Zachos, J., M. Pagani, L. Sloan, E. Thomas, and K. Billups (2001), Trends, rhythms, and aberrations in global climate 65 Ma to present, *Science*, *292*, 686–693, doi:10.1126/science.1059412.

Zimmermann, B., D. Porcelli, M. Frank, P. S. Andersson, M. Baskaran, D.-C. Lee, and A. N. Halliday (2009), Hafnium isotopes in Arctic Ocean water, *Geochim. Cosmochim. Acta*, in press.

J. D. Blum, J. D. Gleason, T. C. Moore Jr., and R. M. Owen, Department of Geological Sciences, University of Michigan, Ann Arbor, MI 48109, USA. (jdgleaso@umich.edu)

B. A. Haley, Leibniz Institute of Marine Sciences at University of Kiel (IFM-GEOMAR), D-24118 Kiel, Germany.

D. J. Thomas, Department of Oceanography, Texas A&M University, College Station, TX 77843, USA.